

Development of global temperature and pH calibrations based on bacterial 3-hydroxy fatty acids in soils

Pierre Véquaud¹, Sylvie Derenne¹, Alexandre Thibault², Christelle Anquetil¹, Giuliano Bonanomi³, Sylvie Collin¹, Sergio Contreras⁴, Andrew Nottingham⁵, Pierre Sabatier⁶, Norma Salinas⁷, Wesley Phillip Scott⁸, Josef P. Werne⁸, Arnaud Huguet¹

¹Sorbonne Université, CNRS, EPHE, PSL, UMR METIS, Paris, 75005, France

²Antea Group, Innovation Hub, 803 boulevard Duhamel du Monceau, Olivet, 45160, France

³Dipartimento di Agraria, Università di Napoli Federico II, via Università 100, Portici, NA, 80055, Italy

⁴Laboratorio de Ciencias Ambientales (LACA), Departamento de Química Ambiental, Facultad de Ciencias & Centro de Investigación en Biodiversidad y Ambientes Sustentables (CIBAS), Universidad Católica de la Santísima Concepción, Casilla 297, Concepción, Chile

⁵School of Geosciences, University of Edinburgh, Crew Building, Kings Buildings, Edinburgh EH9 3FF United Kingdom

⁶Univ. Savoie Mont Blanc, CNRS, EDYTEM, Le Bourget du Lac, 73776, France

⁷Instituto de Ciencias de la Naturaleza, Territorio y Energías Renovables, Pontificia Universidad Católica del Perú, Av. Universitaria 1801, San Miguel, Lima 32, Peru

⁸Department of Geology and Environmental Science, University of Pittsburgh, Pittsburgh, PA 15260, USA

Correspondence to: Arnaud Huguet (arnaud.huguet@sorbonne-universite.fr)

Abstract. 3-hydroxy fatty acids (3-OH FAs) with 10 to 18 C atoms are membrane lipids mainly produced by Gram-negative bacteria. They have been recently proposed as temperature and pH proxies in terrestrial settings. Nevertheless, the existing correlations between pH/temperature and indices derived from 3-OH FA distribution (RIAN, RAN₁₅ and RAN₁₇) are based on a small soil dataset (ca. 70 samples) and only applicable regionally. The aim of this study was to investigate the applicability of 3-OH FAs as mean annual air temperature (MAAT) and pH proxies at the global level. This was achieved using an extended soil dataset of 168 topsoils distributed worldwide, covering a wide range of temperatures (5°C to 30°C) and pH (3 to 8). The response of 3-OH FAs to temperature and pH was compared to that of established branched GDGT-based proxies (MBT'_{5Me}/CBT). Strong linear relationships between 3-OH FA-derived indices (RAN₁₅, RAN₁₇ and RIAN) and MAAT/pH could only be obtained locally, for some of the individual transects. This suggests that these indices cannot be used as paleoproxies at the global scale using simple linear regression models, in contrast with the MBT'_{5Me} and CBT. However, strong global correlations between 3-OH FA relative abundances and MAAT/pH were shown by using other algorithms (multiple linear regression, k-NN and random forest models). The applicability of the three aforementioned models for paleotemperature reconstruction was tested and compared with the MAAT record from a Chinese speleothem. The calibration based on the random forest model appeared to be the most robust. It generally

a supprimé: k-NN and random forest

a supprimé:

50 showed similar trends with previously available records and highlighted known climatic events
51 poorly visible when using local 3-OH FA calibrations. Altogether, these results demonstrate
52 the potential of 3-OH FAs as paleoproxies in terrestrial settings.

53

54 **Keywords:** 3-hydroxy fatty acids; branched GDGTs; soils; global calibration; temperature and
55 pH proxy

56

57

1. Introduction

Investigating past climate variations is essential to understand and predict future environmental changes, especially in the context of global anthropogenic change. Direct records of environmental parameters are available for the last decades, the so-called "instrumental" period. Beyond this period, proxies can be used to obtain indirect information on environmental parameters. A major challenge is to develop reliable proxies which can be applied to continental environments in addition to marine ones. Indeed, available proxies have been mainly developed and used in marine settings, as the composition and mechanism of formation of marine sedimentary cores is less complex than in continental settings, which are highly heterogeneous. Several environmental proxies based on organic (e.g. the alkenone unsaturation index ($U^{k_{37}}$; Brassell et al., 1986) and inorganic (Mg/Ca ratio and $^{18}O/^{16}O$ ratio of foraminifera; Emiliani, 1955; Erez and Luz, 1983) fossil remains were notably developed for the reconstruction of sea surface temperatures.

Some of the existing proxies are based on membrane lipids synthesized by certain microorganisms (Eglinton and Eglinton, 2008; Schouten et al., 2013). These microorganisms are able to adjust the composition of their membrane lipids in response to the prevailing environmental conditions in order to maintain an appropriate fluidity and to ensure the optimal state of the cellular membrane (Singer and Nicolson, 1972; Sinensky, 1974; Hazel and Williams, 1990; Denich et al., 2003). The structure of glycerol dialkyl glycerol tetraethers (GDGTs), which are membrane lipids biosynthesized by archaea and some bacteria, is especially known to be related to environmental conditions. Archaeal GDGTs are constituted of isoprenoid alkyl chains ether-linked to glycerol, whereas bacterial GDGTs are characterized by branched alkyl chains instead of isoprenoid ones. The latter compounds are ubiquitous in terrestrial (Weijers et al., 2007; Peterse et al., 2012; De Jonge et al., 2014; Naafs et al., 2017) and aquatic environments (Peterse et al., 2009; Tierney and Russell, 2009; Sinninghe Damsté et al., 2009; Loomis et al., 2012; Peterse et al., 2015; Weber et al., 2015). These branched GDGTs (brGDGTs) are produced by still unidentified bacteria, although some of them may belong to the phylum *Acidobacteria* (Sinninghe Damsté et al., 2011, 2014, 2018). The analysis of brGDGTs in a large number of soils distributed worldwide showed that the relative distribution of these compounds is mainly related to mean annual air temperature (MAAT) and soil pH (Weijers et al., 2007; Peterse et al., 2012; De Jonge et al., 2014). Despite improvements in brGDGT analytical methods and development of refined calibration models (De Jonge et al., 2014; Dearing Crampton-Flood et al., 2020), the Root Mean Square Error (RMSE) associated

a mis en forme : Français (France)

Code de champ modifié

a supprimé:

Code de champ modifié

a supprimé: ;

a supprimé: Peterse et al., 2009; Tierney and Russell, 2009; Damsté et al., 2009

95 with MAAT reconstruction using the global brGDGT calibrations in soils remains high (>4°C).
96 Thus, development of new molecular proxies, independent of and complementary to brGDGTs,
97 is essential to improve the reliability of temperature reconstructions in such settings.

98 Recent studies have unveiled the potential of another family of [bacterial](#) lipids – 3-
99 hydroxy fatty acids (3-OH FAs) – for temperature and pH reconstructions in terrestrial (Wang
100 et al., 2016, 2018; Huguet et al., 2019) and marine (Yang et al., 2020) settings. 3-OH FAs with
101 10 to 18 carbon atoms are specifically produced by Gram-negative bacteria and are bound to
102 the lipopolysaccharide (LPS) by ester or amide bonds (Wollenweber et al., 1982; Wollenweber
103 and Rietschel, 1990). Three types of 3-OH FAs can be distinguished, with either *normal* chains
104 or branched chains, *iso* or *anteiso*.

105 The analysis of 3-OH FAs in soils showed that [the ratio of C₁₅ or C₁₇ anteiso 3-OH](#)
106 [FA to normal C₁₅ or C₁₇ 3-OH FA \(RAN₁₅ and RAN₁₇ indices, respectively\)](#), were negatively
107 correlated with MAAT along the three mountains investigated so far: Mts. Shennongjia (China;
108 Wang et al., 2016), Rungwe and Majella (Tanzania and Italy, respectively; Huguet et al., 2019).
109 This suggests that Gram-negative bacteria producing these fatty acids [respond to colder](#)
110 temperatures with an increase in *anteiso*-C₁₅/C₁₇ vs. *n*-C₁₅/C₁₇ 3-OH FAs, in order to maintain
111 a proper fluidity and optimal state of the bacterial membrane, the so-called homeoviscous
112 adaptation mechanism (Sinensky, 1974; Hazel and Eugene Williams, 1990). Nevertheless, the
113 relationships between RAN₁₅ and MAAT along the three mountain transects showed the same
114 slopes but different intercepts (Wang et al., 2016; Huguet et al., 2019), suggesting that regional
115 [relations may be more adapted to apply RAN₁₅ as a temperature proxy in soils](#). In contrast, a
116 significant calibration between RAN₁₇ and MAAT could be established using combined data
117 from the three mountain regions (Wang et al., 2016; Huguet et al., 2019).

118 Another index, [defined as the cologarithm of the sum of anteiso and iso 3-OH FAs](#)
119 [divided by the sum of normal homologues \(RIAN index\)](#), was shown to be strongly negatively
120 correlated with soil pH along the three aforementioned mountains (Wang et al., 2016; Huguet
121 et al., 2020), reflecting a general relative increase in normal homologues compared to branched
122 (*iso* and *anteiso*) ones with increasing pH. This mechanism was suggested to reduce the
123 permeability and fluidity of the membrane for the cell to cope with lower pH (Russell et al.,
124 1995; Denich et al., 2003; Beales, 2004).

125 3-OH FA indices were recently applied for the first time to the reconstruction of the
126 temperature and hydrological changes over the last 10,000 years in a speleothem from China
127 (Wang et al., 2018), showing the potential of 3-OH FAs as independent tools for environmental
128 reconstruction in terrestrial settings. A very recent study based on marine sediments from the

a supprimer: the

a supprimer: , defined as the ratio of C₁₅ or C₁₇ anteiso 3-OH FA to normal C₁₅ or C₁₇ 3-OH FA,

a supprimer: similarly

a supprimer: also

a supprimer: calibrations

a supprimer: the RIAN,

136 North Pacific Ocean suggested that the distribution of 3-OH FAs could also be used to
137 reconstruct sea surface temperature (Yang et al., 2020).

138 Even though these results are promising, the linear regressions between pH/MAAT and
139 3-OH FA indices in terrestrial environments are still based on a rather small dataset (ca. 70 soil
140 samples; Wang et al., 2016; Huguet et al., 2019). The aim of this study was to investigate the
141 applicability of 3-OH FAs as MAAT and pH proxies at the global level using an extended soil
142 dataset and refined statistical tools. 3-OH FA distribution from 54 soils was determined in four
143 globally distributed altitudinal transects (Tibet, Italy, Peruvian Andes and Chile) and was
144 combined with data previously published by Wang et al. (2016; Mt Shennongjia, China),
145 Huguet et al. (2019; Mt. Rungwe, Tanzania and Mt. Majella, Italy) and Véquaud et al. (2021;
146 Mts. Lautaret-Bauges, France), leading to a total of 168 samples. In addition to linear
147 regressions, non-parametric, machine learning models were used to improve the global
148 relationships between 3-OH FA distribution and MAAT/pH and present the advantage of taking
149 into account non-linear environmental influences, in line with the intrinsic complexity of the
150 environmental settings. Finally, these new models were tested and compared by applying them
151 to a speleothem archive (Wang et al., 2018) representing to date the only available MAAT
152 record derived from 3-OH FA proxies in continental setting. As brGDGTs are the only
153 microbial organic proxies which can be used for temperature and pH reconstructions in
154 terrestrial settings so far, they can serve as a reference proxy to understand the temperature and
155 pH dependency of 3-OH FAs analyzed in the same dataset, taking into account the large
156 uncertainties persisting in the global temperature/pH brGDGT calibrations (De Jonge et al.,
157 2014; Dearing Crampton-Flood et al., 2020). 3-OH FAs and brGDGTs have thus been
158 concomitantly analyzed to assess their reliability and complementarity as independent
159 temperature and pH proxies.

160

161

162 2. Material and methods

163 2.1. Soil dataset

164 2.1.1. Study sites

165 The dataset of the present study is comprised of the globally distributed surface soils
166 previously analyzed for brGDGTs and 3-OH FAs and collected along 4 altitudinal transects:
167 Mts. Shennongjia (China; Yang et al., 2015; Wang et al., 2016), Rungwe (Tanzania ; Coffinet

a supprimé: further development of the statistical approaches...

a supprimé: a more developed statistical approach

a supprimé: collected

a supprimé: several

a supprimé: along

a supprimé: elevational

a supprimé: under revision

a supprimé: Even though brGDGT-based MAAT and pH reconstructions still have a relatively large uncertainty, they can serve as a reference to understand the temperature dependency of 3-OH FAs analyzed in the same dataset. So, 3-OH FAs and brGDGTs have been concomitantly analyzed to assess their reliability and complementarity as independent temperature and pH proxies.

a supprimé: Even though reconstruction using the global brGDGT calibrations present large uncertainties, there are widely used as MAAT/pH proxies. They can be considered as a reference proxy and were analyzed concomitantly to 3-OH FAs in the dataset.

a supprimé: .

a supprimé:

et al., 2017; Huguet et al., 2019), Majella (Italy; Huguet et al., 2019) and Lautaret-Bauges (France; Véquaude et al., 2021). This set was extended with surficial soils (0-10 cm) from 4 additional altitudinal transects described below, located in Italy, Tibet, Peru and Chile (Table 1).

a supprimé: under revision

a supprimé: elevational

Soil samples were collected from 13 sites along Mount Pollino in the Calabria region (Italy) between 0 and 2,200 m above sea level (a.s.l.) (Table 1). Mt. Pollino is located in the calcareous Apennine range and is 2,248 m a.s.l. It is framed to the northwest by the Sierra de Prete (2,181 m high) and to the south by the Pollino Abyss. The alpine to subalpine area (above 2,100 m a.s.l.) is characterized by the presence of Mediterranean grasslands (*Festuca bosniaca*, *Carex kitaibeliana*) and the presence of sinkholes (Todaro et al., 2007; Scalercio et al., 2014). The mountainous vegetation (over 1,200 m a.s.l.) is dominated by *Fagus sylvatica* forests and, at the treeline, by scattered *Pinus leucodermis* (Bonanomi et al., 2020). The soil is poorly developed and dominated by calcareous soils. Between 0 to 1,200 m a.s.l (Scalercio et al., 2014 and reference therein), Mt. Pollino is characterized by the presence of *Q. ilex* forests or shrubs. Climate along this mountain is humid Mediterranean, with high summer temperatures and an irregular distribution of rainfall throughout the year with pronounced summer drought (39.5% in winter, 23.7% in spring, 29.2% in autumn, 7.6% in summer; average annual precipitation: 1,570 mm; see Todaro et al., 2007). MAAT is comprised between 7 °C (2,200 m a.s.l) and 18 °C (0 m a.s.l; Scalercio et al., 2014). MAAT along Mt. Pollino was estimated using a linear regression between two MAAT (16°C at 400 m a.s.l and 10°C at 1,600 m a.s.l.) from the meteorological data (Castrovillari station) recorded by Scalercio et al. (2014). The pH of the soils analyzed in the present study ranges between 4.5 and 6.8 (Table 1).

a supprimé: spring, 29.2

Soil samples were collected from 17 sites along along Mount Shegyla between 3,106 and 4,474 m a.s.l. (southeastern Tibet, China), as previously described by Wang et al. (2015). Different climatic zonations are observed along this high-altitude site (2,700 to 4,500 m a.s.l): (i) a mountainous temperate zone between 2,700 and 3,400 m, (ii) a subalpine cold temperate zone between 3,400 and 4,300 m and (iii) a cold alpine zone above 4,300 m. Plant species, such as brown oak (*Q. semecarpifolia*) or common fir (*Abies alba*) are abundant within the mountainous and subalpine levels. In the cold subalpine zone, the Forrest's fir (*Abies georgei* var. *smithii*) is endemic to western China. In the cold alpine zone, coniferous species (*Sabina saltuaria*) as well as species typical of mountainous regions such as *Rhododendron* are observed. MAAT was estimated using a linear regression between 7 measured MAAT from the data recorded by Wang et al. (2015). The average MAAT along the transect is 4.6°C, with a

a supprimé: forest fir

227 minimum of 1.1 °C at ca. 4,500 m a.s.l. and a maximum of 8.9 °C at ca. 3,100 m a.s.l. (Table
228 1). Soil pH ranges between 4.6 and 6.4 (Table 1).

229 Soils were sampled from 14 sites in the Peruvian Andes along the Kosñipata transect,
230 located in south-eastern Peru, in the upper part of the Madre de Dios/Madeira watershed, east
231 of the Andes Cordillera (Nottingham et al., 2015). This transect (190 m to 3,700 m a.s.l) is well-
232 documented and is the object of numerous ecological studies (Malhi et al., 2010; Nottingham
233 et al., 2015). There is a shift in vegetation zonation with increasing elevation, from tropical
234 lowland forest to montane cloud forest and high-elevation ‘Puna’ grassland. The tree line lies
235 between 3,200 and 3,600 m a.s.l. For the 14 sites sampled in this study, the lower 13 sites are
236 forest and the highest site is grassland. The 14 sites are part of a network of 1 ha forest plots
237 (Nottingham et al., 2015); for each 1 ha plot, 0-10 cm surface soil was sampled from 5
238 systematically distributed locations within each 1 ha plot. Mean annual precipitation does not
239 vary significantly with altitude (mean = 2448 mm.y⁻¹, SD = 503 mm.y⁻¹; Rapp and Silman, 2012;
240 Nottingham et al., 2015). MAAT is comprised between 26.4 °C at 194 m altitude and 6.5°C at
241 3644 m altitude (Table 1). The pH is characteristic of acidic soils (3.4 - 4.7; Table 1). Further
242 information on these sites and soils is available in Nottingham et al. (2015).

243 Soil samples were collected from 10 sites between 690 m and 1,385 m a.s.l. from the
244 lake shore (20 to 50 m offshore) of 10 Andean lakes located in Chile (38–39°S) within the
245 temperate forest (Table 1). High-frequency measurements of MAAT over a period of one year
246 are available for the different sampling sites. MAAT is comprised between 5.75°C and 9.2°C.
247 Soil pH ranges between 4.4 and 6.8 (Table 1).

249 2.1.2. pH measurement

250 Following sampling, soils were immediately transported to the laboratory and stored at
251 -20 °C. Soil samples from the Peruvian Andes, Mt. Pollino and Mt. Shegyla were then freeze-
252 dried, ground and sieved at 2 mm. The pH of the freeze-dried samples was measured in
253 ultrapure water with a 1:2.5 soil water ratio. Typically, 10 ml of ultrapure water were added to
254 4 g of dry soil. The soil solution was stirred for 30 min, before decantation for 1 hand pH
255 measurement (Carter et al., 2007).

257 2.2. Lipid analyses

258 BrGDGTs and 3-OH FAs were analyzed in all samples from the Peruvian Andes,
259 Chilean Andes, Mt. Pollino and Mt. Shegyla.

a supprimé:

a supprimé: (every hour)

a supprimé: in situ soil temperature

a mis en forme : Police :Non Italique

2.2.1. 3-OH FA analysis

Sample preparation for 3-OH FA analysis was identical to that reported by Huguet et al. (2019) and Véquaud et al. (2021). Soil samples were subjected to acid hydrolysis (3 M HCl) and extracted with organic solvents. This organic fraction was then rotary-evaporated, methylated in a 1M HCl-MeOH solution at 80 °C for 1 h and separated into three fractions over an activated silica column: (i) 30 ml of heptane/EtOAc (98: 2), (ii) 30 ml of EtOAc and (iii) 30 ml of MeOH. 3-OH FAs contained in the second fraction were derivatized at 70°C for 30 min with a solution of *N,O*- bis(trimethylsilyl)trifluoroacetamide (BSTFA) – Trimethylchlorosilane (TMCS) 99:1 (Grace Davison Discovery Science, USA) before gas chromatography-mass spectrometry (GC-MS) analysis.

3-OH FAs were analyzed with an Agilent 6890N GC-5973N using a Restek RXI-5 Sil MS silica column (60 m × 0.25 mm, i.d. 0.25 µm film thickness), as previously described (Huguet et al., 2019). 3-OH FAs were quantified by integrating the appropriate peak on the ion chromatogram and comparing the area with an internal standard (3-hydroxytetradecanoic acid, 2,2,3,4,4-d5; Sigma-Aldrich, France). The internal standard (0.5 mg/ml) was added just before injection as a proportion of 3 µl of standard to 100 µl of sample, as detailed by Huguet et al. (2019). The different 3-OH FAs were identified based on their retention time, after extraction of the characteristic *m/z* 175 fragment (*m/z* 178 for the deuterated internal standard; cf. Huguet et al., 2019).

The RIAN index was calculated as follows (Wang et al., 2016 ; Eq. 1) in the range C₁₀-C₁₈ :

$$\text{RIAN} = -\log[(I + A)/ N] \quad (1)$$

where I, A, N represent the sum of all *iso*, *anteiso* and *normal* 3-OH FAs, respectively.

RAN₁₅ and RAN₁₇ indices are defined as follows (Wang et al., 2016; Eq. 2 and 3):

$$\text{RAN}_{15} = [\text{anteiso } C_{15}] / [\text{normal } C_{15}] \quad (2)$$

$$\text{RAN}_{17} = [\text{anteiso } C_{17}] / [\text{normal } C_{17}] \quad (3)$$

Analytical errors associated with the calculation of RIAN, RAN₁₅ and RAN₁₇ indices are respectively 0.006, 0.3 and 0.2 based on the analysis of one sample injected nine times during the analysis and five samples injected in triplicates.

a supprimer: s

a supprimer: under revision

a supprimer: (3-hydroxytetradecanoic acid, 2,2,3,4,4-d5; Sigma-Aldrich, France).

a supprimer: 3

a supprimer: 3

a supprimer: 4

a supprimer: 5

a supprimer: 4

a supprimer: 5

2.2.2. brGDGT analysis

Sample preparation for brGDGT analysis was similar to that reported by Coffinet et al. (2014). Briefly, ca. 5-10 g of soil was extracted using an accelerated solvent extractor (ASE 100, Dionex-ThermoScientific, USA) with a dichloromethane (DCM) / methanol (MeOH) mixture (9: 1) for 3×5 min at 100 °C and a pressure of 100 bars in 34 ml cells. The total lipid extract was rotary evaporated and separated into two fractions of increasing polarity on a column of activated alumina: (i) 30 ml of heptane: DCM (9: 1, v:v) ; (ii) 30 ml of DCM: MeOH (1: 1, v:v). GDGTs are contained in the second fraction, which was rotary evaporated. An aliquot (300 µL) was re-dissolved in heptane and centrifuged using an Eppendorf MiniSpin centrifuge (Eppendorf AG, Hamberg, Germany) at 7000 rpm for 1 min.

GDGTs were then analyzed by high pressure liquid chromatography coupled with mass spectrometry with an atmospheric pressure chemical ionisation source (HPLC-APCI-MS) using a Shimadzu LCMS 2020. GDGT analysis was performed using two Hypersil Gold silica columns in tandem (150 mm × 2.1 mm, 1.9 µm; Thermo Finnigan, USA) thermally controlled at 40 °C, as described by Huguet et al. (2019). This methodology enables the separation of 5- and 6-methyl brGDGTs. Semi-quantification of brGDGTs was performed by comparing the integrated signal of the respective compound with the signal of a C₄₆ synthesized internal standard (Huguet et al., 2006) assuming their response factors to be identical.

The MBT'_{5Me} index, reflecting the average number of methyl groups in 5-methyl isomers of GDGTs and considered as related to MAAT, was calculated according to De Jonge et al. (2014; Eq. 4):

$$MBT'_{5Me} = \frac{[Ia+Ib+Ic]}{[Ia+Ib+Ic] + [IIa+IIb+IIc] + [IIIa]}$$

The CBT' index, reflecting the average number of cyclopentyl rings in GDGTs and considered as related to pH, was calculated as follows (De Jonge et al., 2014; Eq. 5):

$$CBT' = \log \left(\frac{[Ic] + [IIa'] + [IIb'] + [IIc'] + [IIIa'] + [IIIb'] + [IIIc']}{[Ia] + [IIa] + [IIb] + [IIc] + [IIIa] + [IIIb] + [IIIc]} \right)$$

The Roman numerals correspond to the different GDGT structures presented in De Jonge et al. (2014). The 6-methyl brGDGTs are denoted by an apostrophe after the Roman numerals for their corresponding 5-methyl isomers. Analytical errors associated with the

a supprimé: ¶
¶

a supprimé: l

a supprimé: l

a supprimé: CBT and

a supprimé: Peterse et al., 2012 ;

a supprimé: Peterse et al., 2012

a supprimé: and 6 respectively

a supprimé: 2

a supprimé: ¶
CBT = - log ($\frac{[Ib] + [IIb + II' b]}{[Ia] + [IIa + II' a]}$) (5) ¶

a mis en forme : Retrait : Première ligne : 0 cm

a supprimé: -

a supprimé: b

a supprimé: b+II'b

a supprimé: '

a supprimé: 6

a supprimé: 2

calculation of MBT'_{SM} and CBT' indices are 0.015 and 0.02, respectively, based on the analysis of three samples in triplicate among the 44 soil samples.

2.3. Statistical analysis

In order to investigate the correlations between environmental variables (pH, MAAT) and the relative abundances of bacterial lipids (brGDGTs and 3-OH FAs) or the indices based on these compounds, pairwise correlation matrices were performed in addition to single or multiple linear regressions. As the dataset is not normally distributed, Spearman correlation was used with a confidence level of 5%.

Principal component analyses (PCA) were performed on the different soil samples to statistically compare the 3-OH FA/brGDGT distributions along the different altitudinal transects. The fractional abundances of the bacterial lipids (3-OH FAs and brGDGTs) were used for these PCAs, with MAAT, pH and location of the sampling site representing supplementary variables, (i.e. not influencing the principal components of the analysis).

Independent models should be used for the development of environmental calibrations, as each of them has its own advantages and limits. Linear regression methods are simple to use but many of them suffer from the phenomenon of regression dilution, as previously noted (Naafs et al., 2017; Dearing Crampton-Flood et al., 2020). That is why other models than ordinary least squares or single/multiple regression were also proposed in this study (cf. section 4.2. for discussion of the models): the the k-nearest neighbor (k-NN) and random forest models. These models are based on machine-learning algorithms, which are built on a proportion of the total dataset (randomly defined, i.e. training dataset) and then tested on the rest of the dataset, considered as independent (test dataset).

The k-NN model is based on the estimation of the mean distances between the different samples. This is a supervised learning method (e.g. Gangopadhyay et al., 2009). A training database composed of N "input-output" pairs is initially constituted to estimate the output associated with a new input x. The method of the k-neighbors takes into account the k training samples whose input is the closest to the new input x, according to a distance to be defined. This method is non-parametric and is used for classification and regression. In k-NN regression, the result is the value for this object, which is the average of the values of the k nearest neighbors. Its constraints lie in the fact that, by definition, if a range of values is more frequent than the others, then it will be statistically predominant among the k closest neighbors. But, in the present case, data selection was performed randomly on the dataset with a stratification

a supprimé:

a supprimé: ,

a supprimé: and

a supprimé: CBT

a supprimé: ,

a supprimé: and

a supprimé: and 0.02

a supprimé: ,

a supprimé: ¶
¶

a supprimé: identify the relationships between MAAT/pH and understand

a supprimé: understand

a supprimé: distribution or the indices derived from these compounds...

a supprimé: elevational

a supprimé: PCAs were performed using

a supprimé: t

a supprimé: used as

a supprimé: data

a supprimé: s

a supprimé: used to perform the PCAs

a supprimé: drawbacks

a supprimé: A weak point of

a supprimé: is that they

a supprimé: (

a supprimé: is

a supprimé: O

a supprimé: used

a supprimé: .

a supprimé: The The first model is the k-nearest neighbour (k-NN) algorithm, which is a supervised learning method (e.g. Gangopadhyay et al., 2009). A training database composed of N "input-output" pairs is initially constituted to estimate the output associated with a new input x. The method of the k-neighbors takes into account the k training samples whose input is the closest to the new input x, according to a distance to be defined. This method is non-parametric and is used for classification and regression. In k-NN regression, the result is the value for this object, which is the average of the values of the k nearest neighbors.

a mis en forme : Retrait : Première ligne : 1,25 cm

a supprimé: u

modality according to the MAAT or the pH to limit the impact of extreme values as detailed below. This allows to overcome this limitation of the k-NN method.

The random forest algorithm is also a supervised learning method used, among other things, for regressions (e.g. Ho, 1995; Breiman, 2001; Denisko and Hoffman, 2018;). This model works by constructing a multitude of decision trees at training time and producing the mean prediction of the individual trees. Decision tree learning is one of the predictive modeling approaches used to move from observations to conclusions about the target value of an item. Decision trees where variables are continuous values are called regression trees.

The training phase required for the random forests, k-NN and multiple linear regression was performed on 75% of the sample set with an iteration of ten cross-validations per model. Data selection was performed randomly on the dataset (with no pre-processing of the individual 3-OH FAs) but with a stratification modality according to the MAAT or the pH to limit the impact of extreme values. Then, the robustness and precision of the different models were tested on the remaining 25 % of samples, considered as an independent dataset. Simple and Multiple linear regressions, PCA, k-NN and random forest models were performed with R software, version 3.6.1 (R Core Team, 2014) using the packages - tidymodels (version 0.1.0)- kkn (version 1.3.1), ranger (version 0.11.2). A web application is available online (<https://athibault.shinyapps.io/paleotools>) for the reconstruction of 3-OH FA-derived MAAT using the machine learning models proposed in the present study.

3. Results

3.1. Distribution of bacterial lipids

3.1.1. 3-OH FAs

3-OH FAs were identified in the whole dataset, representing eight elevation transects and 168 samples (Supplementary table 1; Yang et al., 2015; Wang et al., 2016; Coffinet et al., 2017; Huguet et al., 2019; Véquaud et al., 2021). Their chain lengths range between 8 and 26 C atoms, indicating that these compounds have various origins (bacteria, plants, and fungi; Zelles, 1999; Wang et al., 2016 and reference therein). The homologues of 3-OH FAs with 10 to 18 C atoms are considered to be produced exclusively by Gram-negative bacteria (Wollenweber and Rietschel, 1990; Szponar et al., 2003) and will be the only ones considered in the following. Compounds with an even carbon number and *normal* chains were the most

a mis en forme

a supprimé: The second model is t

a supprimé: , which

a supprimé:

a supprimé: (

a supprimé: Breiman, 2001

a supprimé: Machine-learning models are built on a proportion of the total dataset (randomly defined, i.e. Training dataset) and then tested on the rest of the dataset, considered as independent (test dataset).

a mis en forme : Normal

a supprimé: In order to verify and compare the results of the different models proposed in this study, the values of R², RMSE, variance of the residuals, mean absolute error (MAE) and the upper and lower limits of MAAT and pH estimates were presented.

a supprimé: under revision

477 abundant 3-OH FAs in all samples (mean 67.9 % of the total 3-OH FAs, Standard Deviation
478 (SD) 6.8%), with a predominance of the *n*-C₁₄ homologue (21.9%, SD 3.23%; Fig. 1). *Iso* (mean
479 22.9%, SD 5.01%) and *anteiso* (mean 6.33 %, SD 1.79%) isomers were also present. It must be
480 noted that *anteiso* isomers were only detected for odd carbon-numbered 3-OH FAs (Yang et
481 al., 2015; Wang et al., 2016; Coffinet et al., 2017; Huguet et al., 2019).

482 The distribution of 3-OH FAs in the soils of the different altitudinal transects did not
483 show a large variability (Fig. 1). Thus, there was no major difference in the relative abundances
484 of most of the 3-OH FAs (*i*-C₁₁, *a*-C₁₁, *n*-C₁₁, *i*-C₁₂, *a*-C₁₃, *n*-C₁₃, *i*-C₁₄, *n*-C₁₅, *i*-C₁₆, *a*-C₁₇ and
485 *n*-C₁₇) between the 8 study sites, even though slight differences could be observed for some
486 compounds as detailed below. For example, the Peruvian samples were characterized by higher
487 average proportions of *n*-C₁₈ 3-OH FA and lower contribution of the *n*-C₁₀ and *n*-C₁₂
488 homologues than those from the other transects. Soils from Mt. Shegyla were characterized by
489 lower average proportions of *n*-C₁₄ 3-OH FAs and higher abundances of *i*-C₁₇ compounds
490 compared to the other transects (Fig. 1).

491
492 3.1.2. *brGDGTs*

493 The relative abundances of *brGDGTs* were compared between the same transects as
494 for 3-OH FAs, representing a total of 168 samples. The 5- and 6-methyl isomers were separated
495 in most of the samples (Fig. 2; Sup. Table 2), except in older dataset, i.e. soils from Mt. Rungwe
496 (Coffinet et al., 2014, 2017). *BrGDGT data from Mt. Rungwe will not be further considered in*
497 *this study.*

498 The *brGDGT* distribution was dominated by acyclic compounds (Ia, IIa, IIa', IIIa,
499 IIIa') which represent on average ca. 83.4% of total *brGDGTs* (SD = 14.5%; Fig. 2). The
500 tetramethylated (Ia-c; mean 39.3%, SD of 20.5%) and the pentamethylated (IIa-c; 44.8%, SD
501 12.8%) *brGDGTs* were predominant over the hexamethylated ones (IIIa-c; Fig. 2). The 5-
502 methyl isomers were on average present in a higher proportion (mean 71.9%, SD 23.4%) than
503 the 6-methyl compounds (Fig. 2).

504 High variability of the *brGDGT* distribution was observed among the different
505 transects. The relative abundance of *brGDGT* Ia was much higher in the Peruvian soils (mean
506 83%, SD 12.6%) than in the other transects (mean between 17.3% and 61.7%; Fig. 2). The 5-
507 methyl isomers were more abundant than the 6-methyl isomers for all sites except for Mt.
508 Pollino (mean 5-methyl = 44%, SD=11.7%) and Mt. Majella (mean 5-methyl = 33.7 %, SD =
509 5.5%; Fig. 2).

510

a mis en forme : Français (France)
Code de champ modifié

a supprimé: 3
a supprimé:)
a supprimé:
a supprimé: s
a supprimé: s
a déplacé (et inséré) [1]
a supprimé: Sup. (Tables 2, 3 and Sup. Fig. 1)
a mis en forme : Anglais (États-Unis)
a supprimé: and Shennongjia (Yang et al., 2015: Sup. tables 2, 3 and Sup. Fig. 1).
a déplacé vers le haut [1]: Sup. tables 2, 3 and Sup. Fig. 1)
a supprimé: 4
a supprimé: 4.7
a supprimé: 37.4
a supprimé:)
a supprimé: 21.4
a supprimé: 45.2
a supprimé: 13.5

3.2. 3-OH FA and brGDGT-derived indices

3.2.1. 3-OH FA

The RIAN index roughly varied by an order of magnitude among the eight elevation transects (Table 1). The RIAN index ranged from 0.37 to 0.67 for the Peruvian Andes, 0.23 to 0.56 for Mt. Shegyla, 0.15 to 0.34 for Mt. Pollino, 0.21 to 0.53 for the Chilean Andes, 0.26 to 0.80 for Mt. Rungwe (Huguet et al., 2019), 0.16 to 0.46 for Mt. Majella (Huguet et al., 2019), 0.20 to 0.69 for Mt. Shennongjia (Wang et al., 2016) and 0.13 to 0.56 for the French Alps (Véquaude et al., 2021).

The RAN₁₅ varied greatly among the different sites (Table 1). It was in the same range along Mts. Rungwe (1.04-5.73) and Majella (0.68-6.43; Huguet et al., 2019). In contrast, its upper limit was higher for Mts. Shennongjia (0.67-10.77; Wang et al., 2016), Shegyla (4.07-12.17), Pollino (2.41-10.26), the Peruvian Andes (2.45-13.77) and the French Alps (1.44-12.26). The range of variation in RAN₁₅ was narrower for the Chilean Andes (3.82-6.40).

The RAN₁₇ values were similar among the different altitudinal transects (Table 1), ranging from 1.72 to 3.90 along Mt. Shegyla, 0.68 to 6.43 along Mt. Majella (Huguet et al., 2019), 1.19 to 4.54 along Mt. Pollino, 1.91 to 4.25 for the Chilean Andes and 1.12 to 3.57 along Mt. Shennongjia (Wang et al., 2016). The range of RAN₁₇ values was narrower for Mt. Rungwe (0.33-1.62; Huguet et al., 2019) and the Peruvian Andes (0.61-2.39) and wider for the French Alps (0.89-6.42; Véquaude et al., 2021) compared to the other sites.

3.2.2. brGDGT

The range of variation in the MBT'_{5Me} index was homogeneous along most transects (0.32-0.63; Table 1), except the Peruvian Andes, with higher values (0.58-0.98; Table 1). Regarding the CBT' index, it showed similar ranges along Chilean Andes (-2.28 to -0.32) and Mt. Shegyla (-2.39 to -0.35; Table 1). This index showed different ranges of variations along the other altitudinal transects: Mts. Shennongjia (-1.18 to 0.50; Yang et al., 2015), Pollino (-0.24 to 0.43) and Peruvian Andes (-1.91 to -1.09). Finally, The CBT' values varied within a narrow range along Mt. Majella (0.23-0.59; Huguet et al., 2019) and within a wide range along the French Alps (-2.29 to 0.52; Véquaude et al., 2021).

a supprimé: (Véquaude et al., under revision).

a supprimé: under revisio

a supprimé: n

a supprimé: —Saut de page—

a supprimé: ;

a supprimé:

a supprimé: Peruvian Andes (0.97-1.81)

a supprimé: 0.76-

a supprimé: ;

a supprimé: 1.87

a supprimé: elevational

a supprimé: on the one hand and along

a supprimé: 0.14

a supprimé: ;

a supprimé: -1.43

a supprimé: Rungwe (0.16-1.01; Coffinet et al., 2017) and

a supprimé: 0.28

a supprimé: ;

a supprimé: -1.09

a supprimé: ;

a supprimé: on the other hand.

a supprimé: 1

a supprimé: ;

a supprimé: -

a supprimé: 74

a supprimé: 0.25-2.23

a supprimé: ;

a supprimé: under revision

a supprimé: ¶

3.3. Principal component analysis and clustering of 3-OH FA and brGDGT distribution

Principal component analyses were performed to refine the comparison of bacterial lipid distribution (3-OH FAs and brGDGTs) among the different altitudinal transects. 3.3.1. 3-OH FA

The first two axes of the 3-OH FA PCA explained 39.1% of the total variance in the dataset (Fig. 3a). Dimension 1 (23.9%) opposed samples from Mt. Pollino in the right quadrant to Peruvian soils and samples from Mt. Shennongjia. Dimension 2 (15.2%) especially separated individuals from Chile and Mt. Rungwe. The Wilks' test showed that the location of the sampling sites was the best variable discriminating the distribution of the individuals in the PCA.

Principal component analysis performed on the temperature (RAN₁₅, RAN₁₇) and pH (RIAN) indices derived from 3-OH FAs showed that most of the variance was carried by the first two axes of the PCA (Axis 1 = 56.09%; Axis 2 = 35.29%; Supp. Fig. 2). The first axis was highly correlated with the RAN₁₅ (r = 0.87) and RAN₁₇ (r = 0.93) as well as with MAAT (r = -0.67), while Axis 2 showed strong correlations with the RIAN (r = 0.96) and pH (r = -0.61). The PCA allowed visualizing relationships at the scale of the whole dataset, between MAAT and RAN₁₅ and RAN₁₇ (r = -0.61; r = -0.64 respectively) and between pH and RIAN (r = -0.53).

3.3.2. brGDGT

The first two axes of the brGDGT PCA explained 57.7% of the total variance in the dataset (Fig. 3b). Dimension 1 (42.6%) strongly discriminated soils from Mt. Majella and, to a lesser extent, Mt. Pollino, in the right quadrant from those from Mt. Shengyla, Peruvian Andes and Chilean Andes in the left quadrant. Mts Majella and Pollino were also discriminated negatively along dimension 2 (15.1%). Samples from Mts. Shennongjia and Lautaret-Galibier were distributed over the entire PCA. As for the 3-OH FAs, Wilks' test showed that the location of the sampling sites was the best variable discriminating the distribution of the brGDGTs in the PCA.

4. Discussion

4.1. 3-OH FA and brGDGT-derived proxies

Previous studies conducted on soils from individual altitudinal transects revealed (1) local linear relationships between MAAT/pH and 3-OH FA indices and (2) the potential for

a mis en forme : Normal, Aucun(e), Sans numérotation ni puces

a supprimé: elevational

a supprimé: ¶

a mis en forme : Police :Italique, Masqué

a supprimé: inertia

a supprimé: inertia

a supprimé: ¶

a mis en forme : Normal, Sans numérotation ni puces

a mis en forme : Police :Italique, Masqué

a supprimé: 65.3

a supprimé: inertia

a supprimé: 35.60

a supprimé: Rungwe

a supprimé: Majella

a supprimé: and

a supprimé: The former two sites

a supprimé: 29.7

a supprimé: Concerning Mts Shennongjia and Lautaret-Galibier, s...

a supprimé: —Saut de page—

a supprimé: ¶

a mis en forme : Police :Couleur de police : Couleur personnalisée(RVB(0;0;10))

combined calibrations using simple linear regressions (Wang et al., 2016; Huguet et al., 2019; Véquaud et al., 2021). In the present study, the existence of linear relationships between 3-OH FA-derived indices and environmental variables was further investigated using an extended soil dataset and the corresponding results were compared with those derived from the brGDGTs used as an established reference proxy.

a supprimé: under revision

a supprimé: proxies

a supprimé: ,

a supprimé: and well-studied

4.1.1. Relationships between pH and bacterial lipid-derived proxies

The relationship between RIAN and pH was investigated along each of the altitudinal transects (Fig. 4a; Sup. Table 3). No significant linear relationship was obtained for the Peruvian Andes, Mts. Rungwe, Pollino and Majella (Huguet et al., 2019) and weak to moderate correlations were observed along Mts. Shegyla and Lautaret-Bauges ($R^2 = 0.29-0.46$; Sup. Table 3). In contrast, strong regressions between RIAN and pH were observed along Mt. Shennongjia ($R^2 = 0.71$) and in Chilean Andes ($R^2 = 0.66$). A weak linear relationship between RIAN and pH ($R^2=0.34$; $RMSE = 0.99$; $p = 7.39 \times 10^{-17}$) was also obtained when considering the 168 samples for the eight elevation transects altogether. Therefore, our results confirm the general influence of pH on the relative abundance of 3-OH FAs (Huguet et al., 2019) but suggest that strong linear correlations between RIAN and pH can only be obtained (i) at a local level and (ii) only for some of the sites.

a supprimé: 4

a supprimé: 4

a supprimé: 27

a supprimé: 8.63

a supprimé: 4

As previously suggested (Huguet et al., 2019), the absence or weakness of linear correlations between RIAN and pH may be at least partly due to the small range of variation of pH (<2 units) along some mountains, such as Mts. Rungwe, Majella, and the Peruvian Andes (Fig. 4a; Table 1, Huguet et al., 2019). Transects for the Peruvian Andes and Mt. Majella were also characterized by the absence of relationships between pH and the brGDGT-derived CBT' index, supporting the hypothesis that low pH ranges limit the potential of obtaining linear relationships between indices based on bacterial lipids and pH. Nevertheless, the existence of a narrow pH range was not the only limiting factor in obtaining a strong linear regression between RIAN and pH. Indeed, MAAT rather than soil pH was the dominant driver of soil bacterial diversity and community composition for the Peruvian transect (using 16S rRNA sequencing (Nottingham et al., 2018); and using phospholipid fatty acids (Whitaker et al., 2014)), consistent with the weak correlation between soil pH and bacterial lipids. The weakness of the RIAN-pH relationship may also be partly due to the heterogeneity of soils encountered along a given altitudinal transect, representing specific microenvironments and to the large diversity of bacterial communities in soils from different elevations (Siles and Margesin, 2016). The distribution of 3-OH FAs varies greatly among Gram-negative bacterial species (Bhat and

a supprimé: ,

a supprimé: s

a supprimé: and Rungwe

a supprimé: The 3-OH FA distribution strongly varied from a Gram-negative bacterial species to another

688 Carlson, 1992) which may account for the significant variability in RIAN values observed in
689 soils from a given transect. Altogether, these results suggest that linear models are not the most
690 suitable for establishing a global calibration between RIAN and pH in soils.

691 Concerning GDGTs, moderate to strong relationships between brGDGT-derived CBT_z
692 index and pH were observed along 5 of the 7 altitudinal transects investigated (Fig. 4b; Sup.
693 Table 3). All the individual linear relationships between CBT_z and pH, where present, had
694 similar slopes and ordinates and share (for most of the samples) the same 95% confidence
695 intervals (p-value <0.5). This resulted in a strong linear relationship between CBT_z index and
696 pH values for the dataset ($R^2 = 0.68$; RMSE = 0.71; $n = 140$), which is weaker than the global
697 calibration ($R^2 = 0.85$; RMSE = 0.52; $n = 221$) proposed by De Jonge et al. (2014).↓

698 The discrepancy in relationships between temperature and brGDGTs and 3-OH FAs
699 might partly be due to differences in the relative abundance of these lipids among bacterial
700 communities. The brGDGTs are produced by a more restricted and less diverse number of
701 bacterial species than 3-OH FAs, which are arguably biosynthesized by a large diversity of
702 Gram-negative bacteria species (e.g. Wakeham et al., 2003; Zelles et al., 1995; Zelles, 1999).
703 So far, only bacteria from the *Acidobacteria* phylum were identified as putative brGDGT
704 producers in soils (Sinninghe Damsté et al., 2018). The hypothetical lower diversity of brGDGT
705 producers, in contrast with 3-OH FAs might explain the more homogenous response and lower
706 scatter of the relationships between pH and CBT_z index. Moreover, the CBT_z index is a ratio
707 based on a restricted number of compounds, representing the direct dependence of the degree
708 of cyclisation of bacterial GDGTs on pH. Conversely, the RIAN index is calculated from the
709 relative abundances of all the individual 3-OH FAs between C₁₀ and C₁₈ (Wang et al., 2016). It
710 cannot be ruled out that some of the compounds used to calculate the RIAN index are
711 preferentially synthesized, as part of the homeoviscous mechanism, in response to
712 environmental variables other than pH. This calls for a better understanding of the ecology of
713 3-OH FA-producing bacteria and their adaptation mechanisms.

714
715

- a supprimé: among
- a supprimé: within
- a supprimé: , hence a potentially large variability of RIAN values among soils from a given transect
- a supprimé: 4
- a supprimé: 4
- a supprimé: prediction
- a supprimé: whole
- a supprimé: 5
- a supprimé: 3
- a supprimé: 158
- a supprimé: slightly
- a supprimé: 70
- a supprimé: 170
- a supprimé: ,
- a supprimé: (Peterse et al., 2012). was Altogether, these results confirm that, in contrast with the RIAN, the CBT_z index can be applied at a global scale using a simple linear regression model.
- a supprimé: Damste

4.1.2 Relationships between MAAT and bacterial lipid-derived proxies

RAN₁₅ was previously shown to be correlated with MAAT along Mts. Rungwe, Majella and Shennongjia (Wang et al., 2016; Huguet et al., 2019). Moderate to strong linear correlations ($R^2 = 0.49-0.79$) between RAN₁₅ and MAAT were also observed along most of the individual transects investigated (Fig. 5a; Sup. Table 3, except along the Chilean and Lautaret-Bauges transects. The individual correlations do not share the same 95% confidence intervals and even when some of them present similar slopes, the regression lines display significantly different intercepts (p -value > 0.05) (Fig. 5a). This supports the hypothesis of a site-dependent effect of the linear RAN₁₅-MAAT relationship previously made by Huguet et al. (2019).

Similarly to RAN₁₅, RAN₁₇ was moderately to strongly correlated ($R^2 = 0.53-0.81$) with MAAT along 5 out of 8 individual transects (Fig. 5b; Sup. Table 3). The small range of variation in MAAT along the Chilean transect (6.0-9.2 °C) (Table 1), associated with that of the RAN₁₅/RAN₁₇, could explain the lack of a linear relationship between the MAAT and these indices. As for the French Alps (Mts Lautaret-Bauges), the influence of local environmental parameters (pH and to a lesser extent soil moisture and grain size, related to vegetation and soil types, or thermal regimes associated with the snow cover) on 3-OH FA distribution was shown to be predominant over that of MAAT (Véquaud et al., 2021). In contrast with RAN₁₅, the linear regressions between RAN₁₇ and MAAT along Mts. Shegyla, Shennongjia, Rungwe and the Peruvian Andes transects share confidence intervals at 95% and have similar slope and intercept values (p -value < 0.05 ; Fig. 5b; Sup. Table 3), suggesting that RAN₁₇ could be a more effective global proxy for MAAT reconstructions than RAN₁₅.

In order to test the hypothesis that RAN₁₇, rather than RAN₁₅, is a more effective global proxy for MAAT, the global calibrations between RAN₁₅/RAN₁₇ and MAAT based on the entire soil dataset ($n = 168$) were compared. The two linear regressions had similar moderate determination coefficients ($R^2 = 0.37$ and 0.41 for RAN₁₅ and RAN₁₇, respectively) and similar high RMSE (RMSE = 5.46°C and 5.28°C for RAN₁₅ and RAN₁₇, respectively; Sup. Table 4). For all transects (except for the Mt Majella RAN₁₇/MAAT relationship), the individual local regressions between RAN₁₅/RAN₁₇ and MAAT outperformed the proposed global linear calibrations in terms of determination coefficients (0.49-0.81) and RMSE (1.98-3.57 °C; Sup. Table 4), suggesting that local rather than global linear transfer functions based on RAN₁₅ or RAN₁₇ may be more appropriate for paleotemperature reconstructions in soils.

The difficulties in establishing global linear RAN₁₅/RAN₁₇-MAAT calibrations may partly be due to the fact that microbial diversity, especially for 3-OH FA-producing Gram-negative bacteria (Margesin et al., 2009; Siles and Margesin, 2016), can vary greatly from one

a supprimé: ¶

a supprimé: similarly

a supprimé: 4)

a supprimé: prediction

a supprimé: 27

a supprimé: 4

a supprimé: under revision

a supprimé: prediction

a supprimé: 4

soil to another, resulting in variation of the RAN₁₅/RAN₁₇ indices, as also assumed for the RIAN. The strong regional dependence of the 3-OH FA distribution may thus explain the weak correlation between 3-OH FA-derived indices (RAN₁₅, RAN₁₇ and RIAN) and environmental variables (MAAT/pH) at a global level. This regional dependency was further supported by the PCA of the relative abundance of 3-OH FAs across the global dataset, which showed that the individuals were grouped based on the sampling location (Fig. 3a).

In addition to 3-OH FAs, the relationships between brGDGT distribution and MAAT were investigated along the seven transects for which the 5- and 6-methyl brGDGT isomers were separated (Mts Shegyla, Pollino Majella, Lautaret-Bauges, Shennongjia, Peruvian Andes and Chilean Andes). These individual transects showed moderate to strong relationships between MAAT and MBT'_{5Me} (R² 0.35-0.89; Fig. 6 and Sup. Table 3), with similar slopes and ordinates (except for the Peruvian Andes) and shared 95% confidence intervals for most of the samples. A distinct relationship between MBT'_{5Me} and MAAT was observed along the Peruvian Andes and Mt Majella transects (Fig. 6a), as also observed for the RIAN and RAN₁₅ indices (Figs 4a and 5a). The singularity of the Peruvian soils is also visible on the PCA performed on the brGDGT distribution (Fig. 3b), where the samples from this region are pooled very narrowly from the rest of the dataset. This specific trend is difficult to explain, even though the Peruvian Andes are subjected to warmer climatic conditions (Table 1) than the other temperate transects, which may in turn affect the nature of the microbial communities encountered in the soils and the bacteria lipid distribution (Siles and Margesin, 2016; Hofmann et al., 2016; De Jonge et al., 2019).

A moderate linear relationship between MAAT and MBT'_{5Me} ($MAAT = 24.5 \times MBT'_{5Me} - 4.78$; R² = 0.57, RMSE = 3.39 °C, n = 140; Sup. Table 3) was observed after combining the data for the seven aforementioned altitudinal transects. This global relationship follows a similar trend as the calibration proposed by De Jonge et al. 2014 ($MAAT = 31.45 \times MBT'_{5Me} - 8.57$) and is more robust and accurate than those obtained between the RAN₁₅/RAN₁₇ and MAAT (Sup. Table 3). This confirms that the MBT'_{5Me} index can be applied at a global scale using a simple linear regression model as previously shown (De Jonge et al., 2014; Naafs et al., 2017), in contrast with the RAN₁₅ and RAN₁₇ proxies, for which only strong local calibrations with MAAT were found.

As a similar conclusion was obtained for the RIAN-pH proxy, it appears necessary to use more complex models to develop global calibrations between 3-OH FA-derived proxies and MAAT/pH. This novel method allows taking into account the complexity and specificity of each environmental site.

a supprimé: six

a supprimé: 4

a supprimé: 75

a supprimé: prediction

a supprimé: separately

Code de champ modifié

a mis en forme : Français (France)

a mis en forme : Français (France)

a mis en forme : Couleur de police : Texte 1

a supprimé: 6

a supprimé: 65

a supprimé: 04

a supprimé: 4

a supprimé: five

a mis en forme : Couleur de police : Texte 1

a supprimé: 4

a supprimé: was more robust and accurate than those obtained between the RAN₁₅/RAN₁₇ and MAAT (Sup. Table 4).

a supprimé: Furthermore, the relationship between the MBT'_{5Me} and the MAAT obtained in this study ($MAAT = 24.5 \times MBT'_{5Me} - 4.78$) follows a similar trend as the global calibration proposed by De Jonge et al. 2014 ($MAAT = 31.45 \times MBT'_{5Me} - 8.57$).

4.2. Development of new models for the reconstruction of MAAT and pH from 3-OH FA

Several complementary methods were recently used to derive calibrations with environmental parameters from organic proxies. Most calibrations between lipid distribution and environmental variables were based on simple linear regression models, most often the ordinary least square regression (e.g. for brGDGTs: De Jonge et al., 2014; Wang et al., 2016), as it is simple and easy to implement and understand. Other linear models, such as Deming regression (Naafs et al., 2017) or Bayesian regression (Tierney and Tingley, 2014; Dearing Crampton-Flood et al., 2020) were also used. Nevertheless, these single linear regression methods rely on a given index (e.g. MBT'_{5Me} or CBT' for brGDGTs) which is correlated with environmental parameters. This represents a limitation, as the relative distribution of bacterial lipids can be concomitantly influenced by several environmental parameters (e.g. Véquaud et al., 2021) and can also depend on the microbial diversity and sources of these compounds (Parker et al., 1982; Bhat and Carlson, 1992; Zelles, 1999). In contrast, using bacterial relative abundances rather than a single index in the relationships with environmental variables appears less restrictive, and more representative of the environmental complexity. Other models can be used in this way, such as those based on multiple regressions (e.g. Peterse et al., 2012; De Jonge et al., 2014; Russell et al., 2018), describing the relationships between one or several explained variables (e.g. bacterial lipid abundances) and one or several explanatory variables (e.g. MAAT, pH). Multiple regressions can reveal the presence of linear relationships among several known variables but cannot take into account non-linear influences, which may occur in complex environmental settings. This limitation, common to all linear models, can be overcome using non-parametric methods such as some of the machine-learning algorithms (e.g. nearest neighbours or random forest; Dunkley Jones et al., 2020). The reliability of the latter models lies in the fact that they are non-linear, which helps capturing the intrinsic complexity of the environmental setting, and that they avoid the regression dilution phenomenon observed in most linear models. Moreover, their robustness is improved by the fact that they are built on a randomly defined proportion of the total dataset and then tested on the rest of the dataset, considered as independent. Last, these machine-learning algorithms are flexible and are continuously evolving when adding new samples.

As shown in section 4.1., robust global calibrations between 3-OH FA-derived indices (RIAN, RAN₁₅ and RAN₁₇) and MAAT/pH could not be established using a simple linear regression model, contrary to what was observed with brGDGT-derived indices. Therefore,

- a supprimé: ¶
- a supprimé: are
- a supprimé: : (i)
- a supprimé: a simple linear
- a supprimé: : Deming regression (Naafs et al., 2017), ... [1]
- a supprimé: –
- a supprimé: linear
- a supprimé: But these
- a mis en forme ... [2]
- a supprimé: methods are limited by the use of an ind ... [3]
- a supprimé: (1)
- a supprimé: ,
- a supprimé: (2) the fractional abundance of bacterial ... [4]
- a supprimé:
- a supprimé:
- a supprimé: So, other calibration were proposed
- a supprimé: ; or (ii)
- a supprimé: models
- a supprimé: Weijers et al., 2007;
- a supprimé: an
- a supprimé:
- a supprimé: The latter
- a supprimé: The aforementioned models
- a supprimé: can
- a supprimé: To overcome this
- a supprimé:
- a supprimé: of
- a supprimé: parametric models (simple/multiple linea ... [5]
- a supprimé: other approaches were proposed, for exa ... [6]
- a supprimé: use
- a supprimé: models
- a supprimé: to establish environmental calibration
- a supprimé: These machine-learning methods present ... [7]
- a supprimé: in
- a supprimé: a
- a supprimé: with the addition
- a supprimé: of
- a supprimé: A
- a supprimé: previously discussed in this study
- a supprimé: contrary to
- a supprimé: in contrast with
- a supprimé:
- a supprimé: ¶

three different independent and complementary models were tested to potentially establish stronger statistical relationships between 3-OH FA distributions and pH/MAAT at the global level : (i) a parametric model – multiple linear regression; (ii) two non-parametric models – random forest (e.g. Ho, 1995; Denisko and Hoffman, 2018) and k-NN algorithms (e.g. Gangopadhyay et al., 2009). As discussed above, the multiple linear regression model allows the determination of linear relationships between MAAT/pH and the individual relative abundances of 3-OH FAs, instead of indices derived from the latter. As for the two non-parametric models, they present among other things the advantage of taking into account non-linear environmental influences.

The three models, based on a supervised machine learning approach, were applied to the total soil dataset ($n=168$). All the 3-OH FA homologues, whatever their abundance, were included in the models to keep the maximum variability and take into account the specificity and complexity of each altitudinal transect. Indeed, the nature of the individual 3-OH FAs whose fractional abundance is mainly influenced by MAAT/pH may be site-dependent, as previously observed (Véquaud et al., 2021). The performances of these three models were compared with those of the linear calibrations between 3-OH FA-derived indices (RAN₁₅, RAN₁₇, RIAN) and MAAT/pH (Table 2).

4.2.1. Temperature calibrations

The multiple linear regression model yielded a strong relationship between 3-OH FA relative abundances and MAAT (Fig. 7a; Eq.6):

$$\begin{aligned} \text{MAAT } (^{\circ}\text{C}) = & -59.02 \times [nC_{10}] + 102.1 \times [iC_{11}] + 2628.49 \times [aC_{11}] - 165.58 \times [nC_{11}] - 79.799 \times [nC_{12}] \\ & + 89.93 \times [iC_{13}] + 205.06 \times [aC_{13}] - 136.25 \times [nC_{13}] - 309.71 \times [iC_{14}] - 43.16 \times [nC_{14}] \\ & - 9.27 \times [iC_{15}] - 308.53 \times [aC_{15}] + 66.06 \times [nC_{15}] - 60.57 \times [iC_{16}] + 15.53 \times [nC_{16}] + \\ & 13.52 \times [iC_{17}] - 228.76 \times [aC_{17}] - 91.12 \times [nC_{17}] + 42.16 \times [nC_{18}] + 43.71 \end{aligned}$$

$$(n = 168; R^2 = 0.79; \text{RMSE} = 3.0^{\circ}\text{C}) \quad (6)$$

This model, which takes into account the whole suite of 3-OH FAs (C₁₀-C₁₈), presents a higher strength than the global linear relationships between 3-OH FA derived indices and MAAT ($R^2=0.37$ and 0.41 ; $\text{RMSE}=5.5^{\circ}\text{C}$ and 5.3°C for RAN₁₅ and RAN₁₇, respectively; Table 2). The multiple linear regression also improves the accuracy and robustness of MAAT prediction in comparison with single linear relationships, with lower RMSE (3.0°C), variance of the residuals (9.2°C ; Fig. 7d) and mean absolute error (MAE; 2.3°C) than with the RAN₁₅ and RAN₁₇ calibrations (RMSE of 5.5 and 5.3°C ; variance of 29.8 and 27.9°C ; MAE of 4.0 and 3.9°C for RAN₁₅ and RAN₁₇, respectively; Table 2).

- a supprimé: according to the further development of t ... [8]
- a supprimé: other
- a supprimé: (non-parametric, and involving machine ... [9]
- a supprimé:
- a supprimé: (non-parametric models)... As discusse ... [10]
- a supprimé:
- a supprimé: (i.e. the expected response to the model ... [11]
- a supprimé: shown
- a supprimé: it has been shown in previous studies th ... [12]
- a mis en forme ... [13]
- a supprimé: obtained from the same training and tes ... [14]
- a mis en forme ... [15]
- a supprimé: $R^2 = 0.790$; ...ig. 7a; Eq.6): ¶ ... [16]
- a mis en forme ... [17]
- a supprimé: 17.28
- a mis en forme ... [18]
- a supprimé: 274.88
- a mis en forme ... [19]
- a supprimé: 1570.7
- a mis en forme ... [20]
- a supprimé: 4
- a mis en forme ... [21]
- a supprimé: 441.78
- a mis en forme ... [22]
- a supprimé: 1
- a mis en forme ... [23]
- a mis en forme ... [24]
- a supprimé: - 17.68
- a supprimé: 136.19
- a mis en forme ... [25]
- a supprimé: 4
- a supprimé: 266.88
- a mis en forme ... [26]
- a supprimé: 59
- a mis en forme ... [27]
- a supprimé: +...36.67 ... [28]
- a mis en forme ... [29]
- a supprimé: 3
- a mis en forme ... [30]
- a supprimé: 179.19
- a mis en forme ... [31]
- a supprimé: 2
- a mis en forme ... [32]
- a supprimé: +2.71
- a mis en forme ... [33]
- a supprimé: 3
- a mis en forme ... [34]
- a supprimé: 4
- a supprimé: + 50.74
- a mis en forme ... [35]
- a supprimé: 236.81
- a mis en forme ... [36]
- a supprimé: 4
- a mis en forme ... [37]
- a supprimé: 101.98
- a mis en forme ... [38]
- a supprimé: 44.74
- a mis en forme ... [39]
- a supprimé: 68
- a supprimé: 57.22

Similarly to the multiple linear regression model (Fig. 7a), the random forest (Fig. 7b) and k-NN (Fig. 7c) calibrations are characterized by strong determination coefficients (R^2 0.83 and 0.77, respectively). The variance in residuals, MAE and RMSE of the random forest calibration are slightly lower than those of the multiple linear regression and k-NN models (Table 2). An advantage of the random forest algorithm lies in the fact that the weight of the different variables used to define the model can be quantified using the permutation importance method (Breiman, 2001). The α -C₁₅, i -C₁₄, α -C₁₇, n -C₁₂, n -C₁₅, and to a lesser extent n -C₁₇, n -C₁₆ and j -C₁₃ 3-OH FAs were observed to be the homologues predominantly used by the model to estimate MAAT values (Fig. 9a). They include all the 3-OH FAs involved in the calculation of the RAN₁₅ and RAN₁₇ indices, especially the α -C₁₅ homologue. This may explain why linear relationships between the RAN₁₅/RAN₁₇ and MAAT could be established along some of the altitudinal transects investigated until now (Wang et al., 2016; Huguet al., 2019; Véquaud et al., 2021; this study). Nevertheless, other individual 3-OH FAs than those appearing in the calculation of the RAN₁₅ and RAN₁₇ have also a major weight in the random forest model and seem to be influenced by temperature changes, explaining the moderate determination coefficients of the global RAN₁₅/RAN₁₇-MAAT linear relationships observed in this study.

On the whole, the strength and accuracy of the multiple linear regression, k-NN and random forest models are much higher than those based on the RAN₁₅ and RAN₁₇ indices (Table 2). This is likely related to the fact that the three aforementioned models integrate the whole suite of 3-OH FAs homologues (C₁₀ to C₁₈) and thus better capture the complexity of the response of soil Gram-negative bacteria and their lipid distribution to temperature changes than the RAN₁₅ and RAN₁₇ indices. They also present the advantage of increasing the range of temperature which may be predicted by more than 4 °C in comparison with the RAN₁₅ and RAN₁₇ calibrations (Table 2). Indeed, even though the lower limit of MAAT estimates for the three models tested in the present study is slightly higher than those based on the RAN₁₅ and RAN₁₇ indices, the upper limit of the MAAT which can be estimated using the multiple linear regression, random forest and k-NN models is substantially higher (ca. 25 °C) than that based on the RAN₁₅ or RAN₁₇ indices (ca. 17 °C; Table 2).

The three proposed models show the potential of 3-OH FAs as MAAT proxies at the global level, which was not visible using RAN₁₅ and RAN₁₇ indices. The non-parametric models (random forest and k-NN) may benefit from the fact that they take into account the complex, non-linear relationships between environmental parameters and bacterial lipid abundance. This is highlighted when comparing the independent variations of the individual 3-OH FA relative abundances with estimated MAAT for the three proposed models, with non-

a supprimé: ¶

a supprimé: In fact, taking into account for the whole suite of bacterial lipids (here C₁₀-C₁₈ 3-OH FAs) to estimate MAAT values appears to be more representative of the environmental complexity and overcome the use of a single index. Furthermore, the variance of the residuals of the multiple regression is 9.18°C, compared to 26.01°C and 23.43°C for the RAN₁₅ and RAN₁₇ indices respectively (Table 2, Fig. 7d). This proves the robustness and higher accuracy of the multiple regression compared to the use of a simple linear regression, in agreement with the MAE calculated on the 3 models, higher for the RAN₁₅ (4.03°C) and RAN₁₇ (3.85°C) indices than for the multiple regression (2.3°C) (Table 2).¶

a supprimé: ¶

a supprimé: Despite this advantage, the multiple linear regression method is still a parametric model, contrary of random forest and k-NN methods which can take into account possible non linear influences. Both t...he random forest (Fig. 7b) and k-NN (Fig. 7c) models ... [54]

a mis en forme ... [55]

a supprimé: is

a supprimé: 7

a supprimé: is...y includes ... [56]

a mis en forme ... [57]

a mis en forme : Retrait : Première ligne : 1,27 cm

a supprimé: 3

a mis en forme ... [58]

a supprimé: (Figs. 7b, c) reliably predicted MAAT, with even higher determination coefficients ($R^2 = 0.74$ and 0.778 , respectively) and smaller RMSE (2.8°C and 2.73°C, respectively) than simple or multiple linear regressions (Table 2). Similarly, the variance of the residuals and the MAE are much lower for the k-NN and random forest models than for the RAN₁₅ and RAN₁₇ indices (Fig. 7e and f; Table 2). It is worth noting that the variance of the residues of the random forest model is much lower than for the other machine learning models (7.9°C, against about 9°C for the other models; Table 2). This showed a higher accuracy ... [59]

a mis en forme ... [60]

a supprimé: 3

a supprimé: presented

a supprimé: is

a supprimé: ...t ... [61]

a supprimé: ose

a mis en forme : Indice

a supprimé: and

a mis en forme : Indice

a supprimé: 18

a mis en forme : Retrait : Première ligne : 1,43 cm

a mis en forme ... [62]

a supprimé: Nevertheless, the

1319 linear trends for the k-NN and random forest models, in contrast with the multiple linear
1320 regression (Supp. Fig. 2).

1322 4.2.2. pH calibrations

1323 A robust linear relationship between the RIAN and pH could not be obtained from the
1324 whole soil dataset (Fig. 4a; Table 2). In contrast, the multiple regression model provided a
1325 strong correlation between the 3-OH FA fractional abundances and pH (Fig. 8a; Eq. 7):
1326 $pH = -1.45 \times [nC_{10}] - 31.70 \times [iC_{11}] - 162.09 \times [aC_{11}] - 53.22 \times [nC_{11}] - 6.21 \times [nC_{12}] +$
1327 $56.24 \times [iC_{13}] - 2.02 \times [aC_{13}] + 15.10 \times [nC_{13}] + 23.99 \times [iC_{14}] - 4.54 \times [nC_{14}] - 13.79 \times$
1328 $[iC_{15}] - 15.74 \times [aC_{15}] + 1.93 \times [nC_{15}] - 46.29 \times [iC_{16}] - 3.20 \times [nC_{16}] - 1.80 \times [iC_{17}] -$
1329 $8.90 \times [aC_{17}] + 11.46 \times [nC_{17}] - 3.63 \times [nC_{18}] + 7.84$ ($n = 168$; $R^2 = 0.64$; $RMSE = 0.8$). (7)

1330 The random forest (Fig. 8b) and k-NN pH models (Fig. 8c) appeared to be slightly more
1331 robust and accurate than the multiple linear regression (Fig. 8a), as the former two models
1332 presented slightly higher determination coefficients ($R^2 = 0.68$ and 0.70 for k-NN and random
1333 forest, respectively) and slightly lower RMSE (0.7), variance in residuals (0.5) and MAE (0.5)
1334 than the multiple linear regression (Table 2).

1335 As for the MAAT random forest model, the weight of the individual 3-OH FAs in the
1336 pH random forest calibration was determined (Fig. 9b). Three homologues – $i-C_{13}$, $n-C_{15}$, $i-C_{16}$
1337 – had a larger weight in the global pH model than the others (Fig. 9b). This is consistent with a
1338 detailed study of 3-OH FA distribution in soils from the French Alps (Véquaud et al., 2021),
1339 where the $i-C_{13}$ and $i-C_{16}$ 3-OH FAs were observed to be predominantly influenced by pH.
1340 Nevertheless, in addition to the three aforementioned homologues, most of the C_{10} to C_{18} 3-OH
1341 FAs have a non-negligible influence in the random forest pH model, except the $a-C_{15}$ and $i-C_{14}$
1342 compounds (Fig. 9b). This is in line with the definition of the 3-OH FA-based pH index (RIAN)
1343 defined by Wang et al. (2016) which includes the whole suite of 3-OH FAs. These results
1344 suggest that soil Gram-negative bacteria may respond to pH variations by modifying the whole
1345 distribution of 3-OH FAs, even though this needs to be further confirmed by working at the
1346 microbial level.

1347 In any case, in contrast with the RIAN index, the multiple linear regression, k-NN and
1348 random forest models provided strong global calibrations with pH (Fig. 8), as robust as the
1349 global CBT'-pH relationship (Fig. 4b). The three proposed models also increase the range of
1350 pH which can be estimated (~ 4 pH units) in comparison with the RIAN global calibration (~ 3
1351 pH units), further strengthening the potential of these models for soil pH reconstruction. As
1352 MAAT models, the independent variations of the individual 3-OH FA relative abundances with

- a supprimé: 4
- a supprimé: 3 models presented in this study have a ... [63]
- a mis en forme ... [64]
- a mis en forme ... [65]
- a supprimé: ¶
- a mis en forme ... [66]
- a supprimé: Regarding pH, a robust
- a mis en forme ... [67]
- a supprimé: global ... linear relationship between the ... [68]
- a supprimé: moderate
- a supprimé: with ...H ($R^2 = 0.3864$; ...ig. 8a; Eq. 7) ... [69]
- a mis en forme ... [70]
- a supprimé: 2.79
- a supprimé: 49
- a supprimé: 40.69
- a supprimé: 3
- a supprimé: 112.007
- a supprimé: 86
- a supprimé: 31.072
- a supprimé: $2 \dots \times [nC_{11}] - 6.211$... [71]
- a supprimé: $404 \dots [nC_{12}] + 57.095$... [72]
- a mis en forme ... [73]
- a supprimé: 37
- a supprimé: 4.598
- a mis en forme ... [74]
- a supprimé: 17
- a supprimé: 6.784
- a supprimé: 096
- a supprimé: 20.253
- a supprimé: 89
- a supprimé: 3.710
- a supprimé: 1
- a supprimé: 179
- a supprimé: 1
- a supprimé: 21.691
- a supprimé: $38 \dots \times [aC_{15}] + 1.932$... [75]
- a supprimé: $-11.448 \dots [nC_{15}] - 50.177$... [76]
- a supprimé: 88
- a supprimé: 2.668
- a supprimé: 3
- a supprimé: 871
- a supprimé: 799
- a supprimé: 12.571
- a supprimé: 898
- a supprimé: 6.345
- a supprimé: 59
- a supprimé: 4.634
- a supprimé: 0
- a supprimé: –
- a supprimé: 36
- a supprimé: 8.262
- a supprimé: ... ¶ ... [77]
- a supprimé: $38 \dots 4$; $RMSE = 0.89$... [78]
- a supprimé: ... ¶ ... [79]
- a supprimé: k-NN model
- a supprimé: $R^2 = 0.487$ and $RMSE = 0.797$;
- a supprimé: random forest
- a supprimé: did not clearly improve the estimation of ... [80]
- a supprimé: aforementioned
- a mis en forme ... [81]
- a mis en forme ... [82]

estimated pH highlight non-linear trends for the k-NN and random forest models, in contrast with the multiple linear regression (Supp. Fig. 3), which might favor the use of the two non-parametric models in order to take into account such non-linear influences. The machine-learning MAAT and pH models proposed in this paper are flexible and could be further improved by increasing the number of soil samples analyzed and the representativeness of the different MAAT and pH values within the dataset.

4.3. Paleoclimate application of the new 3-OH FA/MAAT models

The multiple regression, random forest and k-NN models developed for MAAT reconstruction using 3-OH FAs were similar in terms of robustness and precision (Figs. 7a, b, c; Table 2). The performance and validity of these global terrestrial calibrations for paleotemperature reconstructions was thus tested and compared with the MAAT record from a Chinese speleothem (HS4 stalagmite) covering the last 9,000 years BP (Wang et al., 2018). This terrestrial archive was the object of previous paleostudies, thus providing a context for the interpretation of the MAAT data and, to the best of our knowledge, represents the only published application of 3-OH FAs as a paleotemperature proxy in terrestrial settings (Wang et al., 2018). The local comparison of 3-OH FA distributions in the overlying soils and stalagmites and the analyses of bacterial diversity and transport pathways suggested that the 3-OH FAs in the HS4 speleothem were mainly soil-derived (Wang et al., 2018), supporting the application of soil calibrations for MAAT reconstruction from this archive, although not being a paleosoil itself. The first paleoapplication of 3-OH FAs (Wang et al., 2018) on this speleothem relied on a local calibration between the RAN₁₅ index and MAAT proposed by Wang et al. (2016) using soils from Mt. Shennogjia. The MAAT estimates derived from our global soil calibrations were compared with those obtained from this local soil calibration (Wang et al., 2016).

4.3.1 Comparison of the multiple linear regression, k-NN and random forest global MAAT calibrations

The multiple regression model (Eq. 6; Fig. 7a) yielded MAAT estimates ranging between -35 and 22.8 °C over the last 9,000 years (Supp. Fig. 4). The temperature minimum (-35°C) observed at 560 yrs BP can be considered as an outlier, with a significantly lower MAAT estimate than those provided by the other samples. After having ignored this apparent outlier, the MAAT range over the last 9,000 years was comprised between 3.2°C and 22.8°C, with

a supprimé: 5

a supprimé: ¶

¶

¶

a supprimé: In order to complete this first study which highlights the usefulness of 3-OH FAs as MAAT and pH proxies at the global level, it is possible to observe the independent variations of the relative abundances of each 3-OH FA when estimating MAAT or pH values (Supp. Fig. 4 and 5). It appears from this statistical approach that the use of the non-parametric models k-NN and Random forest, allow to highlight non-linear variations of the abundances of 3-OH FAs according to the estimated values of MAAT or pH. This seems to prove the major interest of using non-parametric models, revealing non-linear influences and variations, able to summarize the environmental complexity.¶ (... [90])

a supprimé: ————— Saut de page ————— (... [91])

a supprimé: ¶

a mis en forme : Anglais (États-Unis)

a supprimé: random forest,

a supprimé: and

a mis en forme : Retrait : Première ligne : 1,5 cm

a supprimé:

a supprimé: for MAAT reconstruction based on 3-O (... [92])

a supprimé: applicability

a supprimé: and based on the RAN₁₅ index (Fig. 9a: (... [93])

a supprimé: To the best of our knowledge, t

a supprimé: .

a supprimé:

a supprimé: Wang et al. (2018), which was the objec (... [94])

a supprimé: , it has been proved that

a supprimé: are

a supprimé: from the overlying soils

a supprimé: 2016;

a supprimé: This allowed the application of our glob (... [95])

a supprimé:

a supprimé: was based

a supprimé: 3-OH FAs soil

a mis en forme : Indice

a supprimé: (

a supprimé: ,

a supprimé: This allow a direct comparison of

a supprimé: c

a supprimé: previously presented

a supprimé: soil

a supprimé: random forest and

a supprimé: 6

1796 temperature shifts of up to 15 °C within very short periods of time. The observed range of
 1797 MAAT and large variations in temperature over such short periods appear far too excessive, as
 1798 the expected amplitude of MAAT during the Holocene is expected to be up to ca. 2-3 °C (Liu
 1799 et al., 2014). This highly questions the reliability of the multiple linear regression model for
 1800 MAAT reconstruction from this archive.

1801 MAAT estimates derived from the k-NN calibration ranged between 6.5 and 19.7 °C
 1802 over the last 9,000 years (Supp. Fig. 4). Abrupt shifts in MAAT of more than 10 °C were
 1803 observed between 2,000 and 4,000 yrs BP. Such variations, higher than the RMSE of the
 1804 calibration, appear excessive for the Holocene period, as previously discussed for the multiple
 1805 regression model. The bias in MAAT estimates may be due to the intrinsic definition of the k-
 1806 NN model, which is better suited for uniformly distributed datasets. This is not the case here,
 1807 as the individual transects heterogeneously cover a wide range of temperatures. The application
 1808 of a global calibration at the local scale – that of the HS4 stalagmite – using the k-NN method
 1809 and based on the similarities among samples, thus does not appear appropriate. Such a
 1810 calibration might be improved by extending the dataset with samples more equally distributed
 1811 across a wider range of global climatic gradients.

1812 Finally, the random forest model yielded MAAT estimates between 10.6 and 19.3°C,
 1813 i.e. a much smaller range than the k-NN algorithm and multiple regression model (Supp. Fig.
 1814 4). The amplitude of the shifts observed between 2,000 and 4,000 yrs BP was ca. 4°C, which is
 1815 climatically more consistent than the variations obtained with the k-NN method and multiple
 1816 regression model, even though these large variations in MAAT over such short periods of time
 1817 still appear too excessive. Furthermore, the application of the global random forest calibration
 1818 roughly provided similar temperature trends as those derived from the local RAN₁₅ calibration
 1819 by Wang et al. (2018; Fig. 10), despite some largest oscillations for the global model. These
 1820 results suggest that the random forest calibration is more reliable than the multiple regression
 1821 and k-NN ones. This can be explained by the intrinsic definition of the random forest algorithm,
 1822 which averages the results of several independent models (so-called decision trees), thus
 1823 reducing the variance and thus the forecast error on the final model. This is also in line with the
 1824 slightly higher accuracy of the random forest calibration compared with the other two models
 1825 (Table 2), as previously discussed. In contrast, the multiple regression calibration was the less
 1826 performant of the three models on the investigated archive. This may be related to its parametric
 1827 nature and the fact that it does not take into account the natural non-linear variations on 3-OH
 1828 FA fractional abundances highlighted by the random forest and k-NN models (Supp. Figs. 2
 1829 and 3).

- a supprimé: ¶
- a supprimé: 8
- a supprimé: 14.3
- a supprimé: Fig.
- a supprimé: 9b
- a supprimé: 5
- a supprimé: These large variations in MAAT over such short periods of time are
- a supprimé: and
- a supprimé: ,
- a supprimé: as the expected amplitude of MAAT during
- a supprimé:
- a supprimé: is expected to be up to ca. 2-3 °C (Liu et al., 2014)
- a supprimé: because
- a supprimé: method
- a supprimé: , which
- a supprimé: Concerning the multiple regression, MAAT estimates ranged between -35 and 22.8 °C over the last 9,000 years (Supp. Fig. 6). The temperature minimum (-35°C) observed 560 yrs BP appears to be an outlier, at odds with the magnitudes of MAAT variations observed during the Holocene. If this apparent outlier is ignored, the estimated MAAT vary between 3.2°C and 22.8°C during the Holocene. As for the k-NN model, these large variations in MAAT over such short periods of time, during the entire Holocene, appear excessive (Liu et al., 2014). Furthermore, we have seen in section 4.2 that the multiple regression does not allow for potential non-linear influences, which seem to have been highlighted (Supp. Fig. 4). ¶
- a supprimé: T
- a supprimé: 11.1
- a supprimé: 7
- a supprimé: Fig. 9c
- a supprimé: 3
- a supprimé: if
- a supprimé: also
- a mis en forme : Anglais (États-Unis)
- a supprimé: two
- a supprimé: 4
- a supprimé: 5
- a supprimé: supported by the fact that, in the previous section, we shown that the random forest model presented the best RMSE and the least variance in residuals (Fig 8 e, Table 2).

1874 In conclusion, the three models proposed in this study, especially the random forest,
 1875 have potential for MAAT reconstruction, even though the application to a well-known
 1876 paleoclimate archive showed their limitations. This highlights the importance of testing new
 1877 calibrations on well-characterized archives to investigate their reliability.

1879 4.3.2. Comparison of the global random forest and local RAN₁₅ calibrations for MAAT 1880 reconstruction

1881 The random forest model was observed to be the most reliable of the three proposed
 1882 global MAAT calibrations (Fig. 7). To go further, we compared the temperature record derived
 1883 from our global random forest calibration with that derived from the local MAAT/RAN₁₅
 1884 transfer function proposed by Wang et al. (2016; Fig. 10). The application of the local RAN₁₅
 1885 calibration to the HS4 stalagmite yielded an average MAAT of ca. 18.4 °C over the most recent
 1886 part of the record (last 800 yrs; Fig. 10), consistent with the MAAT of 18 °C recorded *in situ*
 1887 by a temperature logger (Hu et al., 2008; Wang et al., 2018). In contrast, absolute MAAT
 1888 estimates derived from the random forest model were on average 14.2 °C over the last 800 yrs
 1889 and were generally lower than those obtained from the local RAN₁₅ calibration over the whole
 1890 record. Altogether, these results suggest that the random forest model tends to underestimate
 1891 absolute MAAT, in contrast with the RAN₁₅ calibration proposed by Wang et al. (2016). This
 1892 discrepancy may be due the fact that the calibration proposed in the present study is based on a
 1893 global dataset, with samples subject to a large variety of environmental and climatic conditions,
 1894 whereas the RAN₁₅-MAAT transfer function by Wang et al. (2016) was constructed using soil
 1895 samples from a regional altitudinal transect, located at only 120 km distance from the stalagmite
 1896 site (Wang et al., 2018).

1897 Even though the local calibration by Wang et al. (2016) provides more accurate
 1898 absolute MAAT values than the present global random forest model, as it could be expected,
 1899 both calibrations roughly generate similar qualitative MAAT trends over time. A regular slight
 1900 decrease in temperature of ca. 1 °C was observed between 9,000 and ca. 1,000 yrs BP based on
 1901 the local RAN₁₅ calibration (Fig. 10a; Wang et al., 2018). This general decreasing trend was
 1902 also visible when using the random forest model, but with larger oscillations and mainly
 1903 between 9,000 and 4,000 yrs BP, in agreement with the general trend recorded by the $\delta^{18}\text{O}$
 1904 record (mixture of temperature and hydrological signals, Wang et al., 2018) of the HS4
 1905 stalagmite (Fig. 10c,d; Hu et al., 2008). In addition, both the global random forest, local RAN₁₅
 1906 calibrations and the $\delta^{18}\text{O}$ record allowed the identification of several climatic events in the
 1907 Northern hemisphere, in agreement with the reconstructed total solar irradiance (TSI,

a supprimé: ¶
 In the previous section, we highlighted the potential of three models using machine learning to build MAAT calibrations from the relative abundances of 3-OH FAs. The three proposed models appeared then to perform better than the RAN₁₅ and RAN₁₅ indices, as well as accurate and robust.

a supprimé: Nevertheless, t

a supprimé:

a supprimé: of the models on a known

a mis en forme : Anglais (États-Unis)

a mis en forme : Anglais (États-Unis)

a supprimé: ic

a mis en forme : Anglais (États-Unis)

a supprimé: has highlighted

a supprimé: a

a mis en forme : Anglais (États-Unis)

a mis en forme : Anglais (États-Unis)

a mis en forme : Anglais (États-Unis)

a supprimé: of these models (amplitudes of MAAT variations, outliers...).

a supprimé: crucial

a supprimé: shows

a mis en forme : Anglais (États-Unis)

a supprimé:

a supprimé: on a known and studied archive in order to prove its reliability. Furthermore, this first global calibration is proposed on a relatively small number of soil samples, and compared to a reconstitution based on a local calibration based on geographically close samples (120 km). One ... [96]

a supprimé: ¶

a mis en forme : Retrait : Première ligne : 0 cm

a supprimé: W

a supprimé:

a supprimé: s

a supprimé: the

a supprimé: and

a supprimé: the one

a supprimé: (

a supprimé: ,

a supprimé:) (

a supprimé: 9

a supprimé: A

a supprimé: 9

a supprimé: 2008;Wang

a supprimé: 7

a supprimé: 9a

a supprimé: 9

Steinhilber et al., 2009, Fig. 10e). Thus, both models highlighted, with slightly different amplitudes, the Medieval Warm Period (800-1000 years BP) and Little Ice Age (LIA; 200-500 years BP) periods (Mann et al., 2008; Ljungqvist, 2010; Wang et al., 2018). The LIA event is particularly well represented by the global random forest calibration, in line with the decrease in the TSI (Fig. 10c,e) associated with a relative increase in the $\delta^{18}\text{O}$ of HS4 carbonates (dry/cool event, Wang et al., 2018). Before the MWP, the global random forest calibration shows slight oscillations, which can be assumed to be representative of TSI variations between 500 and 1,300 yrs BP. Similarly, an important cooling event, well correlated with a significant decrease in the TSI (Fig. 10a, c, e), was recorded by the two calibrations at 1300 yr BP.

The global random forest calibration also highlighted two cooling events, poorly represented by the local RAN_{15} calibration: one at ca. 4,200 yrs BP ago and, to a lesser extent, another one between 2,800 and 3,000 yrs BP (Bond et al., 2001; Mayewski et al., 2004). The event at 4,200 yrs BP is consistent with the $\delta^{18}\text{O}$ and solar irradiance records and is referenced in the literature as the "4.2 kiloyear event" (deMenocal, 2001). This intense drought event was suggested to have had a major impact on different civilizations (collapses, migrations; Gibbons, 1993; Staubwasser et al., 2003; Li et al., 2018; Bini et al., 2019). Thus, in some parts of China, the production of rice fields sharply decreased during this period, leading to a decrease in population (Gao et al., 2007).

Both calibrations additionally shows a cooling period between 4,000 yrs and 3,200 yrs BP, more pronounced based on the global random forest model, followed by another cooling between 3,200 years BP and 3,000 yrs BP. This cooling period is consistent with the trends derived from $\delta^{18}\text{O}$ and solar irradiance records. It culminates with a cold episode at 3000 yrs BP, also known as Late Bronze Age Collapse (Kaniewski et al., 2013). Indeed, this cold episode, combined with droughts, may have led to a decrease in agricultural production in China, contributing to the degradation of trade routes and ultimately to the collapse of Bronze Age civilizations (Weiss, 1982; Knapp and Manning, 2016). Last, the global random forest calibration also highlights two additional cold events, between 5,600 and 5,900 yrs BP, as well as around 7,100 yrs BP, corresponding to solar irradiance minima (Bond et al., 2001; Mayewski et al., 2004) and which are not as clearly visible with the local RAN_{15} calibration by Wang et al. (2016).

The first application of the random forest calibration to a natural archive shows the potential of 3-OH FAs as paleotemperature proxies at a global scale, as known and documented climatic events were recorded, with a similar RMSE (2.8 °C; Table 2) as that of the local calibration by Wang et al. (2.6 °C; 2016). This RMSE is also much lower than the one related

a supprimé: 9e

a supprimé: 9

a supprimé: large

a supprimé: 9

a supprimé: one between 2,800 and 3,000 yrs BP and another

a supprimé: and another

a supprimé: The global random forest

a supprimé: 000

a supprimé: with

a supprimé: a

a supprimé: (-1°C/800 years)

a supprimé: between 4,000 yrs and 3,200 yrs BP, followed by an abrupt cooling

a supprimé: (-2°C/200 years).

a supprimé: , represented more accurately by the random forest model than by the local RAN_{15} calibration,

a mis en forme : Indice

a supprimé: .

a supprimé: 2.6 -

a supprimé: 7

2017 to the latest global MAAT-brGDGT calibrations ($> 4^{\circ}\text{C}$; De Jonge et al., 2014; Naafs et al.,
2018 2017; Dearing Crampton-Flood et al., 2020), even though the latter are based on a larger number
2019 of soil samples than the global 3-OH FA model proposed in the present study. In summary, we
2020 demonstrate that 3-OH FAs are promising and effective temperature proxies for terrestrial
2021 settings, complementary to, and independent of, the brGDGTs, and also highlight the usefulness
2022 of non-parametric models using machine learning, especially the random forest algorithm, to
2023 establish global MAAT calibrations. We expect that analyses of 3-OH FAs in a larger number
2024 of globally distributed soils will further improve the accuracy and robustness of the global
2025 random forest calibration for paleotemperature reconstruction.

a supprimé: .

2026

2027

2028 5. Conclusions

a supprimé: ¶

a mis en forme : Retrait : Première ligne : 0 cm

2029 3-OH FAs have been recently proposed as environmental proxies in terrestrial settings,
2030 based on local studies. This study investigated for the first time the applicability of these
2031 compounds as MAAT and pH proxies at the global scale using an extended soil dataset across
2032 a series of globally distributed elevation transects ($n = 168$). Strong linear relationships between
2033 3-OH FA-derived indices (RAN_{15} , RAN_{17} and RIAN) and MAAT/pH could only be obtained
2034 locally, for some individual transects, suggesting that these indices cannot be used as
2035 paleoproxies at the global scale through this kind of model. Other algorithms (multiple linear
2036 regression, k-NN and random forest models) were tested and, in contrast with simple linear
2037 regressions, provided strong global correlations between MAAT/pH and 3-OH FA relative
2038 abundances. The applicability of these three models for paleotemperature reconstruction was
2039 tested and compared with the MAAT record from the unique available record: a Chinese
2040 speleothem. The calibration based on the random forest model appeared to be the most robust
2041 and showed similar trends to previous reconstructions and known Holocene climate variations.
2042 Furthermore, the global random forest model highlighted documented climatic events poorly
2043 represented by the local RAN_{15} calibration. This new global model is promising for
2044 paleotemperature reconstructions in terrestrial settings and could be further improved by
2045 analyzing 3-OH FAs in a larger number of globally distributed soils. This study demonstrates
2046 the major potential of 3-OH FAs as MAAT/pH proxies in terrestrial environments through the
2047 different models presented and their application for paleoreconstruction.

a supprimé: the k-NN and random forest

2048

2049 **Data availability.** All data are available in the Supplementary tables.

2053

2054 **Author contributions.** P.V. performed the lipid and statistical analyses and wrote a first draft
2055 of the paper., A.H. and S.D. supervised the work of P.V. and corrected the first draft, P.V. and
2056 A.T. developed the different models, G.B., A.N., W.P.S., N.S., J.P.W. and S.C. provided
2057 samples and/or associated data, and all the co-authors reviewed and commented on the paper.

2058

2059 **Competing interests.** The authors declare that they have no conflict of interest.

2060

2061 **Acknowledgments.** We thank Sorbonne Université for a PhD scholarship to P.V. and the Labex
2062 MATISSE (Sorbonne Université) for financial support. The EC2CO program (CNRS/INSU –
2063 BIOHEFFECT/MICROBIEN) is thanked for funding of the SHAPE project. A.H. and S.C. are
2064 grateful for funding of the ECOS SUD/ ECOS ANID #C19U01 project. We are grateful to
2065 Jérôme Poulenard for discussions on soil characteristics, and for comments on the manuscript.
2066 We thank Dr. Juntao Wang and Prof. Jinzheng He for having provided soils from Mt. Shengyala.

2067

[We thank the reviewers for their comments which helped in improving the manuscript.](#)

2068 References

- 2069 Beales, N.: Adaptation of Microorganisms to Cold Temperatures, Weak Acid Preservatives,
2070 Low pH, and Osmotic Stress: A Review, 3, 1–20, <https://doi.org/10.1111/j.1541->
2071 [4337.2004.tb00057.x](https://doi.org/10.1111/j.1541-4337.2004.tb00057.x), 2004.
- 2072 Bhat, U. R. and Carlson, R. W.: A new method for the analysis of amide-linked hydroxy fatty
2073 acids in lipid-As from gram-negative bacteria, *Glycobiology*, 2, 535–539,
2074 <https://doi.org/10.1093/glycob/2.6.535>, 1992.
- 2075 Bini, M., Zanchetta, G., Persoiu, A., Cartier, R., Catala, A., Cacho, I., Dean, J. R., Di Rita, F.,
2076 Drysdale, R. N., Finné, M., Isola, I., Jalali, B., Lirer, F., Magri, D., Masi, A., Marks, L., Mercuri,
2077 A. M., Peyron, O., Sadori, L., Sicre, M.-A., Welc, F., Zielhofer, C., and Brisset, E.: The 4.2 ka
2078 BP Event in the Mediterranean region : an overview, 15, 555–577, 2019.
- 2079 Bonanomi, G., Zotti, M., Mogavero, V., Cesarano, G., Saulino, L., Rita, A., Tesei, G.,
2080 Allegrezza, M., Saracino, A., and Allevato, E.: Climatic and anthropogenic factors explain the
2081 variability of *Fagus sylvatica* treeline elevation in fifteen mountain groups across the
2082 Apennines, *Forest Ecosystems*, 7, 5, <https://doi.org/10.1186/s40663-020-0217-8>, 2020.
- 2083 Bond, G., Kromer, B., Beer, J., Muscheler, R., Evans, M. N., Showers, W., Hoffmann, S., Lotti-
2084 Bond, R., Hajdas, I., and Bonani, G.: Persistent Solar Influence on North Atlantic Climate
2085 During the Holocene, 294, 2130–2136, <https://doi.org/10.1126/science.1065680>, 2001.
- 2086 Brassell, S. C., Eglinton, G., Marlowe, I. T., Pflaumann, U., and Sarnthein, M.: Molecular
2087 stratigraphy: a new tool for climatic assessment, 320, 129–133,
2088 <https://doi.org/10.1038/320129a0>, 1986.
- 2089 Breiman, L.: Random Forests, *Machine Learning*, 45, 5–32,
2090 <https://doi.org/10.1023/A:1010933404324>, 2001.
- 2091 Carter, M. R., Gregorich, E. G., and Gregorich, E. G.: Soil Sampling and Methods of Analysis,
2092 CRC Press, <https://doi.org/10.1201/9781420005271>, 2007.
- 2093 Coffinet, S., Hugué, A., Williamson, D., Fosse, C., and Derenne, S.: Potential of GDGTs as a
2094 temperature proxy along an altitudinal transect at Mount Rungwe (Tanzania), *Organic*
2095 *Geochemistry*, 68, 82–89, <https://doi.org/10.1016/j.orggeochem.2014.01.004>, 2014.
- 2096 Coffinet, S., Hugué, A., Pedentchouk, N., Bergonzini, L., Omuombo, C., Williamson, D.,
2097 Anquetil, C., Jones, M., Majule, A., Wagner, T., and Derenne, S.: Evaluation of branched
2098 GDGTs and leaf wax n-alkane δ^2H as (paleo) environmental proxies in East Africa,
2099 *Geochimica et Cosmochimica Acta*, 198, 182–193, <https://doi.org/10.1016/j.gca.2016.11.020>,
2100 2017.
- 2101 De Jonge, C., Hopmans, E. C., Zell, C. I., Kim, J.-H., Schouten, S., and Sinninghe Damsté, J.
2102 S.: Occurrence and abundance of 6-methyl branched glycerol dialkyl glycerol tetraethers in
2103 soils: Implications for palaeoclimate reconstruction, *Geochimica et Cosmochimica Acta*, 141,
2104 97–112, <https://doi.org/10.1016/j.gca.2014.06.013>, 2014.
- 2105 De Jonge, C., Radujković, D., Sigurdsson, B. D., Weedon, J. T., Janssens, I., and Peterse, F.:
2106 Lipid biomarker temperature proxy responds to abrupt shift in the bacterial community

a supprimé: Damsté, J. S. S., Ossebaer, J., Abbas, B., Schouten, S., and Verschuren, D.: Fluxes and distribution of tetraether lipids in an equatorial African lake: Constraints on the application of the TEX86 palaeothermometer and BIT index in lacustrine settings, *Geochimica et Cosmochimica Acta*, 73, 4232–4249, <https://doi.org/10.1016/j.gca.2009.04.022>, 2009.¶
Damsté, J. S. S., Rijpstra, W. I. C., Hopmans, E. C., Weijers, J. W. H., Foesel, B. U., Overmann, J., and Dedysh, S. N.: 13,16-Dimethyl Octacosanedioic Acid (iso-Diabolic Acid), a Common Membrane-Spanning Lipid of Acidobacteria Subdivisions 1 and 3, *Appl. Environ. Microbiol.*, 77, 4147–4154, <https://doi.org/10.1128/AEM.00466-11>, 2011.¶
Damsté, J. S. S., Rijpstra, W. I. C., Hopmans, E. C., Foesel, B. U., Wüst, P. K., Overmann, J., Tank, M., Bryant, D. A., Dunfield, P. F., Houghton, K., and Stott, M. B.: Ether- and Ester-Bound iso-Diabolic Acid and Other Lipids in Members of Acidobacteria Subdivision 4, *Appl. Environ. Microbiol.*, 80, 5207–5218, <https://doi.org/10.1128/AEM.01066-14>, 2014.¶
Damsté, J. S. S., Rijpstra, W. I. C., Foesel, B. U., Huber, K. J., Overmann, J., Nakagawa, S., Kim, J. J., Dunfield, P. F., Dedysh, S. N., and Villanueva, L.: An overview of the occurrence of ether- and ester-linked iso-diabolic acid membrane lipids in microbial cultures of the Acidobacteria: Implications for brGDGT paleoproxies for temperature and pH, *Org. Geochem.*, 124, 63–76, <https://doi.org/10.1016/j.orggeochem.2018.07.006>, 2018.¶

2135 composition in geothermally heated soils, *Organic Geochemistry*, 137, 103897,
2136 <https://doi.org/10.1016/j.orggeochem.2019.07.006>, 2019.

2137 Dearing Crampton-Flood, E., Tierney, J. E., Peterse, F., Kirkels, F. M. S. A., and Sinninghe
2138 Damsté, J. S.: BayMBT: A Bayesian calibration model for branched glycerol dialkyl glycerol
2139 tetraethers in soils and peats, *Geochimica et Cosmochimica Acta*, 268, 142–159,
2140 <https://doi.org/10.1016/j.gca.2019.09.043>, 2020.

2141 deMenocal, P. B.: Cultural Responses to Climate Change During the Late Holocene, 292, 667–
2142 673, <https://doi.org/10.1126/science.1059287>, 2001.

2143 Denich, T. J., Beaudette, L. A., Lee, H., and Trevors, J. T.: Effect of selected environmental
2144 and physico-chemical factors on bacterial cytoplasmic membranes, *Journal of Microbiological*
2145 *Methods*, 52, 149–182, [https://doi.org/10.1016/S0167-7012\(02\)00155-0](https://doi.org/10.1016/S0167-7012(02)00155-0), 2003.

2146 Denisko, D. and Hoffman, M. M.: Classification and interaction in random forests, *Proc Natl*
2147 *Acad Sci USA*, 115, 1690–1692, <https://doi.org/10.1073/pnas.1800256115>, 2018.

2148 [Dunkley Jones, T., Eley, Y.L., Thomson, W., Greene, S.E., Mandel, I., Edgar, K., Bendle, J.A., OPTiMAL: a new machine learning approach for GDGT-based palaeothermometry. *Climate of the Past* 16, 2599–2617, 2020.](#)

2151 Eglinton, T. I. and Eglinton, G.: Molecular proxies for paleoclimatology, *Earth and Planetary*
2152 *Science Letters*, 275, 1–16, <https://doi.org/10.1016/j.epsl.2008.07.012>, 2008.

2153 Emiliani, C.: Pleistocene Temperatures, *The Journal of Geology*, 63, 538–578,
2154 <https://doi.org/10.1086/626295>, 1955.

2155 Erez, J. and Luz, B.: Experimental paleotemperature equation for planktonic foraminifera,
2156 *Geochimica et Cosmochimica Acta*, 47, 1025–1031, [https://doi.org/10.1016/0016-7037\(83\)90232-6](https://doi.org/10.1016/0016-7037(83)90232-6), 1983.

2158 Gangopadhyay, S., Harding, B. L., Rajagopalan, B., Lukas, J. J., and Fulp, T. J.: A
2159 nonparametric approach for paleohydrologic reconstruction of annual streamflow ensembles,
2160 45, <https://doi.org/10.1029/2008WR007201>, 2009.

2161 Gao, H., Zhu, C., and Xu, W.: Environmental change and cultural response around 4200 cal. yr
2162 BP in the Yishu River Basin, Shandong, *J GEOGR SCI*, 17, 285–292,
2163 <https://doi.org/10.1007/s11442-007-0285-5>, 2007.

2164 Gibbons, A.: How the Akkadian Empire Was Hung Out to Dry, *Science*, 261, 985,
2165 <https://doi.org/10.1126/science.261.5124.985>, 1993.

2166 Hazel, J. R. and Eugene Williams, E.: The role of alterations in membrane lipid composition in
2167 enabling physiological adaptation of organisms to their physical environment, *Progress in Lipid*
2168 *Research*, 29, 167–227, [https://doi.org/10.1016/0163-7827\(90\)90002-3](https://doi.org/10.1016/0163-7827(90)90002-3), 1990.

2169 Hofmann, K., Lamprecht, A., Pauli, H., and Illmer, P.: Distribution of Prokaryotic Abundance
2170 and Microbial Nutrient Cycling Across a High-Alpine Altitudinal Gradient in the Austrian
2171 Central Alps is Affected by Vegetation, Temperature, and Soil Nutrients, *Microb Ecol*, 72, 704–
2172 716, <https://doi.org/10.1007/s00248-016-0803-z>, 2016.

a supprimé: ¶

- 2174 Hu, C., Henderson, G. M., Huang, J., Xie, S., Sun, Y., and Johnson, K. R.: Quantification of
2175 Holocene Asian monsoon rainfall from spatially separated cave records, *Earth and Planetary*
2176 *Science Letters*, 266, 221–232, <https://doi.org/10.1016/j.epsl.2007.10.015>, 2008.
- 2177 Huguet, A., Coffinet, S., Roussel, A., Gayraud, F., Anquetil, C., Bergonzini, L., Bonanomi, G.,
2178 Williamson, D., Majule, A., and Derenne, S.: Evaluation of 3-hydroxy fatty acids as a pH and
2179 temperature proxy in soils from temperate and tropical altitudinal gradients, *Organic*
2180 *Geochemistry*, 129, 1–13, <https://doi.org/10.1016/j.orggeochem.2019.01.002>, 2019.
- 2181 Huguet, C., Hopmans, E. C., Febo-Ayala, W., Thompson, D. H., Sinninghe Damsté, J. S., and
2182 Schouten, S.: An improved method to determine the absolute abundance of glycerol
2183 dibiphytanyl glycerol tetraether lipids, *Organic Geochemistry*, 37, 1036–1041,
2184 <https://doi.org/10.1016/j.orggeochem.2006.05.008>, 2006.
- 2185 Kaniewski, D., Campo, E. V., Guiot, J., Burel, S. L., Otto, T., and Bacteman, C.: Environmental
2186 Roots of the Late Bronze Age Crisis, *PLOS ONE*, 8, e71004,
2187 <https://doi.org/10.1371/journal.pone.0071004>, 2013.
- 2188 Knapp, A. B. and Manning, S. W.: Crisis in Context: The End of the Late Bronze Age in the
2189 Eastern Mediterranean, 120, 99–149, <https://doi.org/10.3764/aja.120.1.0099>, 2016.
- 2190 Li, C.-H., Li, Y.-X., Zheng, Y.-F., Yu, S.-Y., Tang, L.-Y., Li, B.-B., and Cui, Q.-Y.: A high-
2191 resolution pollen record from East China reveals large climate variability near the
2192 Northgrippian-Meghalayan boundary (around 4200 years ago) exerted societal influence,
2193 *Palaeogeography, Palaeoclimatology, Palaeoecology*, 512, 156–165,
2194 <https://doi.org/10.1016/j.palaeo.2018.07.031>, 2018.
- 2195 Liu, Z., Zhu, J., Rosenthal, Y., Zhang, X., Otto-Bliesner, B. L., Timmermann, A., Smith, R. S.,
2196 Lohmann, G., Zheng, W., and Elison Timm, O.: The Holocene temperature conundrum, *Proc*
2197 *Natl Acad Sci U S A*, 111, E3501–E3505, <https://doi.org/10.1073/pnas.1407229111>, 2014.
- 2198 Ljungqvist, F. C.: A new reconstruction of temperature variability in the extra-tropical northern
2199 hemisphere during the last two millennia, 92, 339–351, <https://doi.org/10.1111/j.1468->
2200 0459.2010.00399.x, 2010.
- 2201 Loomis, S. E., Russell, J. M., Ladd, B., Street-Perrott, F. A., and Sinninghe Damsté, J. S.:
2202 Calibration and application of the branched GDGT temperature proxy on East African lake
2203 sediments, *Earth and Planetary Science Letters*, 357–358, 277–288,
2204 <https://doi.org/10.1016/j.epsl.2012.09.031>, 2012.
- 2205 Malhi, Y., Silman, M., Salinas, N., Bush, M., Meir, P., and Saatchi, S.: Introduction: Elevation
2206 gradients in the tropics: laboratories for ecosystem ecology and global change research, 16,
2207 3171–3175, <https://doi.org/10.1111/j.1365-2486.2010.02323.x>, 2010.
- 2208 Mann, M. E., Zhang, Z., Hughes, M. K., Bradley, R. S., Miller, S. K., Rutherford, S., and Ni,
2209 F.: Proxy-based reconstructions of hemispheric and global surface temperature variations over
2210 the past two millennia, *Proceedings of the National Academy of Sciences*, 105, 13252–13257,
2211 <https://doi.org/10.1073/pnas.0805721105>, 2008.
- 2212 Margesin, R., Jud, M., Tscherko, D., and Schinner, F.: Microbial communities and activities in
2213 alpine and subalpine soils: Communities and activities in alpine and subalpine soils, 67, 208–
2214 218, <https://doi.org/10.1111/j.1574-6941.2008.00620.x>, 2009.

2215 Mayewski, P. A., Rohling, E. E., Curt Stager, J., Karlén, W., Maasch, K. A., David Meeker, L.,
 2216 Meyerson, E. A., Gasse, F., van Kreveld, S., Holmgren, K., Lee-Thorp, J., Rosqvist, G., Rack,
 2217 F., Staubwasser, M., Schneider, R. R., and Steig, E. J.: Holocene climate variability, *Quaternary*
 2218 *Research*, 62, 243–255, <https://doi.org/10.1016/j.yqres.2004.07.001>, 2004.

2219 Naafs, B. D. A., Gallego-Sala, A. V., Inglis, G. N., and Pancost, R. D.: Refining the global
 2220 branched glycerol dialkyl glycerol tetraether (brGDGT) soil temperature calibration, *Organic*
 2221 *Geochemistry*, 106, 48–56, <https://doi.org/10.1016/j.orggeochem.2017.01.009>, 2017.

2222 Nottingham, A. T., Whitaker, J., Turner, B. L., Salinas, N., Zimmermann, M., Malhi, Y., and
 2223 Meir, P.: Climate Warming and Soil Carbon in Tropical Forests: Insights from an Elevation
 2224 Gradient in the Peruvian Andes, 65, 906–921, <https://doi.org/10.1093/biosci/biv109>, 2015.

2225 Nottingham, A. T., Fierer, N., Turner, B. L., Whitaker, J., Ostle, N. J., McNamara, N. P.,
 2226 Bardgett, R. D., Leff, J. W., Salinas, N., Silman, M. R., Kruuk, L. E. B., and Meir, P.: Microbes
 2227 follow Humboldt: temperature drives plant and soil microbial diversity patterns from the
 2228 Amazon to the Andes, 99, 2455–2466, <https://doi.org/10.1002/ecy.2482>, 2018.

2229 Peterse, F., Kim, J.-H., Schouten, S., Kristensen, D. K., Koç, N., and Sinninghe Damsté, J. S.:
 2230 Constraints on the application of the MBT/CBT palaeothermometer at high latitude
 2231 environments (Svalbard, Norway), *Organic Geochemistry*, 40, 692–699,
 2232 <https://doi.org/10.1016/j.orggeochem.2009.03.004>, 2009.

2233 Peterse, F., van der Meer, J., Schouten, S., Weijers, J. W. H., Fierer, N., Jackson, R. B., Kim,
 2234 J.-H., and Sinninghe Damsté, J. S.: Revised calibration of the MBT–CBT paleotemperature
 2235 proxy based on branched tetraether membrane lipids in surface soils, *Geochimica et*
 2236 *Cosmochimica Acta*, 96, 215–229, <https://doi.org/10.1016/j.gca.2012.08.011>, 2012.

2237 Peterse, F., Moy, C. M., and Eglinton, T. I.: A laboratory experiment on the behaviour of soil-
 2238 derived core and intact polar GDGTs in aquatic environments, *Biogeosciences*, 12, 933–943,
 2239 <https://doi.org/10.5194/bg-12-933-2015>, 2015.

2240 [R Core Team, R: A language and environment for statistical computing. R Foundation for](#)
 2241 [Statistical Computing, Vienna, Austria, 2014.](#)

2242 Russell, J. M., Hopmans, E. C., Loomis, S. E., Liang, J., and Sinninghe Damsté, J. S.:
 2243 Distributions of 5- and 6-methyl branched glycerol dialkyl glycerol tetraethers (brGDGTs) in
 2244 East African lake sediment: Effects of temperature, pH, and new lacustrine paleotemperature
 2245 calibrations, *Organic Geochemistry*, 117, 56–69,
 2246 <https://doi.org/10.1016/j.orggeochem.2017.12.003>, 2018.

2247 Russell, N. J., Evans, R. I., ter Steeg, P. F., Hellemons, J., Verheul, A., and Abee, T.:
 2248 Membranes as a target for stress adaptation, *International Journal of Food Microbiology*, 28,
 2249 255–261, [https://doi.org/10.1016/0168-1605\(95\)00061-5](https://doi.org/10.1016/0168-1605(95)00061-5), 1995.

2250 Scalercio, S., Bonacci, T., Mazzei, A., Pizzolotto, R., and Brandmayr, P.: Better up, worse
 2251 down: bidirectional consequences of three decades of climate change on a relict population of
 2252 *Erebia cassioides*, *J Insect Conserv*, 18, 643–650, <https://doi.org/10.1007/s10841-014-9669-x>,
 2253 2014.

a supprimé: ¶

- 2255 Schouten, S., Hopmans, E. C., and Sinninghe Damsté, J. S.: The organic geochemistry of
2256 glycerol dialkyl glycerol tetraether lipids: A review, *Organic Geochemistry*, 54, 19–61,
2257 <https://doi.org/10.1016/j.orggeochem.2012.09.006>, 2013.
- 2258 Siles, J. A. and Margesin, R.: Abundance and Diversity of Bacterial, Archaeal, and Fungal
2259 Communities Along an Altitudinal Gradient in Alpine Forest Soils: What Are the Driving
2260 Factors?, *Microb Ecol*, 72, 207–220, <https://doi.org/10.1007/s00248-016-0748-2>, 2016.
- 2261 Sinensky, M.: Homeoviscous Adaptation—A Homeostatic Process that Regulates the Viscosity
2262 of Membrane Lipids in *Escherichia coli*, *PNAS*, 71, 522–525,
2263 <https://doi.org/10.1073/pnas.71.2.522>, 1974.
- 2264 Singer, S. J. and Nicolson, G. L.: The Fluid Mosaic Model of the Structure of Cell Membranes,
2265 175, 720–731, <https://doi.org/10.1126/science.175.4023.720>, 1972.
- 2266 Sinninghe Damsté, J. S., Rijpstra, W. I. C., Hopmans, E. C., Weijers, J. W. H., Foesel, B. U.,
2267 Overmann, J. and Dedysh, S. N.: 13,16-Dimethyl Octacosanedioic Acid (iso-Diabolic Acid), a
2268 Common Membrane-Spanning Lipid of Acidobacteria Subdivisions 1 and 3, *Appl. Environ.*
2269 *Microbiol.*, 77(12), 4147–4154, doi:10.1128/AEM.00466-11, 2011.
- 2270 Sinninghe Damsté, J. S., Rijpstra, W. I. C., Hopmans, E. C., Foesel, B. U., Wüst, P. K.,
2271 Overmann, J., Tank, M., Bryant, D. A., Dunfield, P. F., Houghton, K. and Stott, M. B.: Ether-
2272 and Ester-Bound iso-Diabolic Acid and Other Lipids in Members of Acidobacteria Subdivision
2273 4, *Appl. Environ. Microbiol.*, 80(17), 5207–5218, doi:10.1128/AEM.01066-14, 2014.
- 2274 Sinninghe Damsté, J. S. S., Rijpstra, W. I. C., Foesel, B. U., Huber, K. J., Overmann, J.,
2275 Nakagawa, S., Kim, J. J., Dunfield, P. F., Dedysh, S. N. and Villanueva, L.: An overview of the
2276 occurrence of ether- and ester-linked iso-diabolic acid membrane lipids in microbial cultures of
2277 the Acidobacteria: Implications for brGDGT paleoproxies for temperature and pH, *Org.*
2278 *Geochem.*, 124, 63–76, doi:10.1016/j.orggeochem.2018.07.006, 2018.
- 2279 Staubwasser, M., Sirocko, F., Grootes, P. M., and Segl, M.: Climate change at the 4.2 ka BP
2280 termination of the Indus valley civilization and Holocene south Asian monsoon variability,
2281 *Geophysical Research Letters*, 30, 1425, <https://doi.org/10.1029/2002GL016822>, 2003.
- 2282 Steinhilber, F., Beer, J., and Fröhlich, C.: Total solar irradiance during the Holocene, 36,
2283 <https://doi.org/10.1029/2009GL040142>, 2009.
- 2284 Szponar, B., Kraśnik, L., Hryniewiecki, T., Gamian, A., and Larsson, L.: Distribution of 3-
2285 Hydroxy Fatty Acids in Tissues after Intraperitoneal Injection of Endotoxin, *Clin Chem*, 49,
2286 1149–1153, <https://doi.org/10.1373/49.7.1149>, 2003.
- 2287 Tierney, J. E. and Russell, J. M.: Distributions of branched GDGTs in a tropical lake system:
2288 Implications for lacustrine application of the MBT/CBT paleoproxy, *Organic Geochemistry*,
2289 40, 1032–1036, <https://doi.org/10.1016/j.orggeochem.2009.04.014>, 2009.
- 2290 Tierney, J. E. and Tingley, M. P.: A Bayesian, spatially-varying calibration model for the
2291 TEX86 proxy, *Geochimica et Cosmochimica Acta*, 127, 83–106,
2292 <https://doi.org/10.1016/j.gca.2013.11.026>, 2014.
- 2293 Todaro, L., Andreu-Hayles, L., D'Alessandro, C., Gutiérrez, E., Cherubini, P., and Saracino,
2294 A.: Response of *Pinus leucodermis* to climate and anthropogenic activity in the National Park

2295 of Pollino (Basilicata, Southern Italy), *Biological Conservation*, 137, 507–519,
 2296 <https://doi.org/10.1016/j.biocon.2007.03.010>, 2007.

2297 Véquaud, P., Derenne, S., Anquetil, C., Collin, S., Poulenard, J., Sabatier, P., and Huguet, A.:
 2298 Influence of environmental parameters on the distribution of bacterial lipids in soils from the
 2299 French Alps: Implications for paleo-reconstructions, *Organic Geochemistry*, 153, 104194,
 2300 <https://doi.org/10.1016/j.orggeochem.2021.104194>, 2021.

2301 Wakeham, S. G., Pease, T. K., and Benner, R.: Hydroxy fatty acids in marine dissolved organic
 2302 matter as indicators of bacterial membrane material, *Organic Geochemistry*, 34, 857–868,
 2303 [https://doi.org/10.1016/S0146-6380\(02\)00189-4](https://doi.org/10.1016/S0146-6380(02)00189-4), 2003.

2304 Wang, C., Bendle, J., Yang, Y., Yang, H., Sun, H., Huang, J., and Xie, S.: Impacts of pH and
 2305 temperature on soil bacterial 3-hydroxy fatty acids: Development of novel terrestrial proxies,
 2306 *Organic Geochemistry*, 94, 21–31, <https://doi.org/10.1016/j.orggeochem.2016.01.010>, 2016.

2307 Wang, C., Bendle, J. A., Zhang, H., Yang, Y., Liu, D., Huang, J., Cui, J., and Xie, S.: Holocene
 2308 temperature and hydrological changes reconstructed by bacterial 3-hydroxy fatty acids in a
 2309 stalagmite from central China, *Quaternary Science Reviews*, 192, 97–105,
 2310 <https://doi.org/10.1016/j.quascirev.2018.05.030>, 2018.

2311 Wang, J.-T., Cao, P., Hu, H.-W., Li, J., Han, L.-L., Zhang, L.-M., Zheng, Y.-M., and He, J.-Z.:
 2312 Altitudinal Distribution Patterns of Soil Bacterial and Archaeal Communities Along Mt.
 2313 Shengyila on the Tibetan Plateau, *Microb Ecol*, 69, 135–145, <https://doi.org/10.1007/s00248-014-0465-7>, 2015.

2315 Weber, Y., De Jonge, C., Rijpstra, W. I. C., Hopmans, E. C., Stadnitskaia, A., Schubert, C. J.,
 2316 Lehmann, M. F., Sinninghe Damsté, J. S., and Niemann, H.: Identification and carbon isotope
 2317 composition of a novel branched GDGT isomer in lake sediments: Evidence for lacustrine
 2318 branched GDGT production, *Geochimica et Cosmochimica Acta*, 154, 118–129,
 2319 <https://doi.org/10.1016/j.gca.2015.01.032>, 2015.

2320 Weijers, J. W. H., Schouten, S., van den Donker, J. C., Hopmans, E. C., and Sinninghe Damsté,
 2321 J. S.: Environmental controls on bacterial tetraether membrane lipid distribution in soils,
 2322 *Geochimica et Cosmochimica Acta*, 71, 703–713, <https://doi.org/10.1016/j.gca.2006.10.003>,
 2323 2007.

2324 Weiss, B.: The decline of Late Bronze Age civilization as a possible response to climatic
 2325 change, *Climatic Change*, 4, 173–198, <https://doi.org/10.1007/BF00140587>, 1982.

2326 Whitaker, J., Ostle, N., Nottingham, A. T., Ccahuana, A., Salinas, N., Bardgett, R. D., Meir, P.,
 2327 and McNamara, N. P.: Microbial community composition explains soil respiration responses to
 2328 changing carbon inputs along an Andes-to-Amazon elevation gradient, 102, 1058–1071,
 2329 <https://doi.org/10.1111/1365-2745.12247>, 2014.

2330 Wollenweber, H. W. and Rietschel, E. T.: Analysis of lipopolysaccharide (lipid A) fatty acids.,
 2331 11, 195–211, 1990.

2332 Wollenweber, H.-W., Broady, K. W., Luderitz, O., and Rietschel, E. T.: The Chemical Structure
 2333 of Lipid A, 124, 191–198, <https://doi.org/10.1111/j.1432-1033.1982.tb05924.x>, 1982.

2334 Yang, H., Lü, X., Ding, W., Lei, Y., Dang, X., and Xie, S.: The 6-methyl branched tetraethers
2335 significantly affect the performance of the methylation index (MBT') in soils from an altitudinal
2336 transect at Mount Shennongjia, *Organic Geochemistry*, 82, 42–53,
2337 <https://doi.org/10.1016/j.orggeochem.2015.02.003>, 2015.

2338 Zelles, L.: Fatty acid patterns of phospholipids and lipopolysaccharides in the characterisation
2339 of microbial communities in soil: a review, *Biol Fertil Soils*, 29, 111–129,
2340 <https://doi.org/10.1007/s003740050533>, 1999.

2341

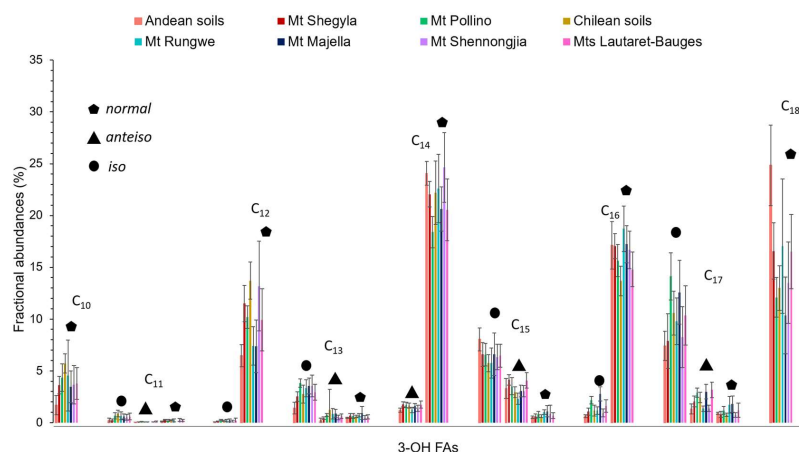


Figure 1. Average distribution of 3-OH FAs along the 8 altitudinal transects investigated in this study. Data from Mts. Majella and Rungwe were taken from Huguet et al. (2019). Data from Mt. Shennongjia were taken from Wang et al. (2016). Data from Mts. Lautaret-Galibier were taken from Véquaud et al. (2021).

a supprimé: under revision

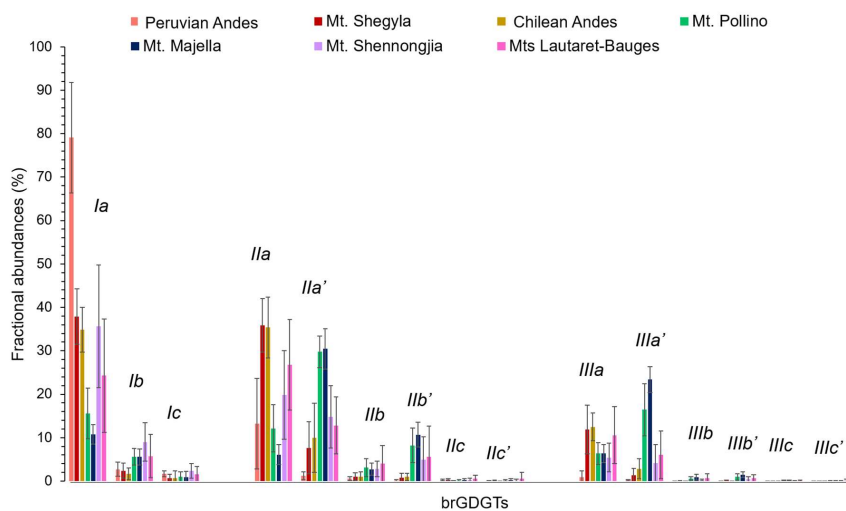


Figure 2. Average distribution of 5- and 6-methyl brGDGTs, along Mts. Shegyla, Pollino Majella, Lautaret-Bauges, Peruvian Andes and Chilean Andes. Data from Mt. Majella were taken from Huguet et al. (2019). [Data from Mt. Shennongjia were taken from Yang et al. \(2015\).](#) [Data from Mts. Lautaret-Galibier were taken from Véquaud et al. \(2021\).](#)

a supprimé: ,

a supprimé:

a supprimé: under revision

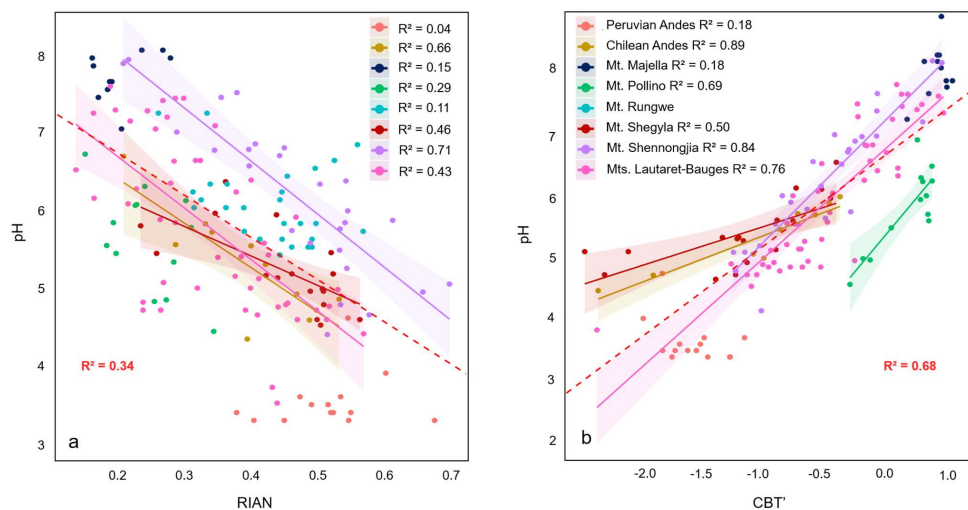


Figure 4. Linear regressions between (a) pH and RIAN and (b) pH and CBT' along the 8 altitudinal transects investigated. Dotted lines represent the 95% [confidence](#) interval for each regression and colored areas represent the 95% confidence interval for each regression. Data for Mts. Majella and Rungwe were taken from Huguet et al. (2019). Data from Mt. Shennongjia were taken from [Yang et al. \(2015\)](#) and [Wang et al. \(2016\)](#). Data from Mts. Lautaret-Galibier were taken from Véquaud et al. (2021). Only significant regressions ($p < 0.05$) are shown.

a supprimé: prediction

a supprimé: Wang et al. (2016).

a supprimé: ,

a supprimé: ,

a supprimé: under revision

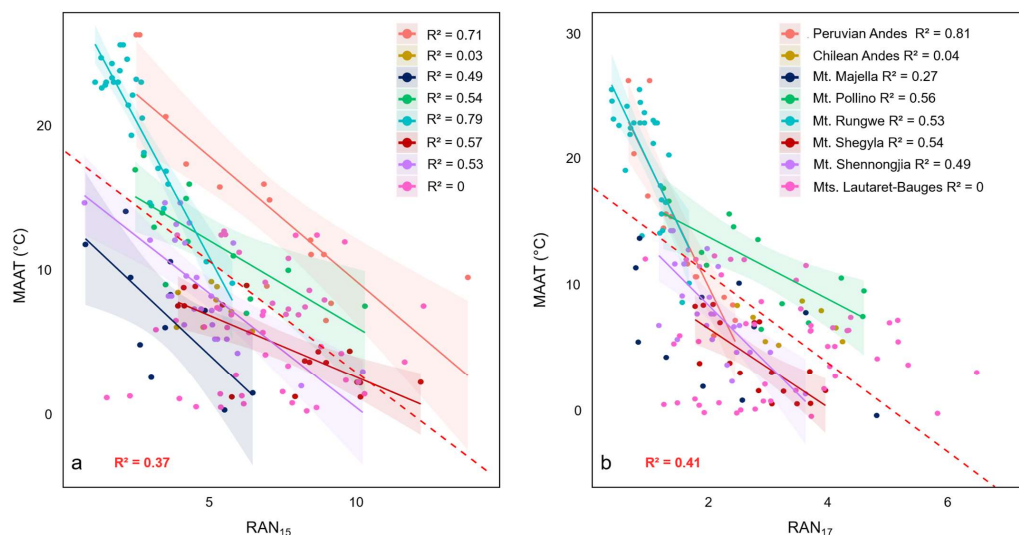


Figure 5. Linear regressions between (a) MAAT and RAN₁₅ and (b) MAAT and RAN₁₇ along the 8 altitudinal transects investigated. Dotted lines represent the 95% confidence interval for each regression and colored areas represent the 95% confidence interval for each regression. Data from Mts. Majella and Rungwe were taken from Huguet et al. (2019). Data from Mt. Shennongjia were taken from Wang et al. (2016). Data from Mts. Lautaret-Galibier were taken from Véquaud et al. (2021). Only significant regressions ($p < 0.05$) are shown.

a ~~supprimé~~: elevational

a ~~supprimé~~: prediction

a ~~supprimé~~: under revision

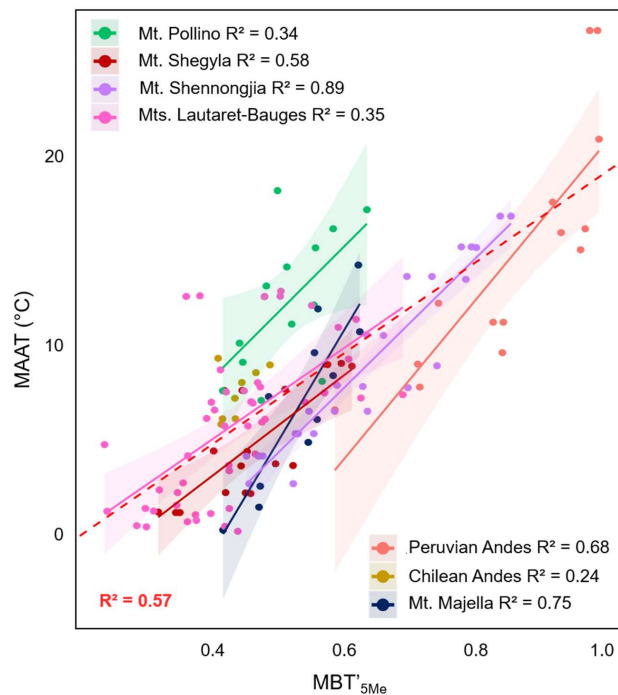


Figure 6. Linear regressions between (a) MAAT and MBT'_{5Me} along 7 of the 8 altitudinal transects investigated. Data from Mt. Rungwe (Coffinet et al., 2014), for which 5- and 6-methyl brGDGTs were not separated, were not included in this graph. Dotted lines represent the 95% confidence interval for each regression and colored areas represent the 95% confidence interval for each regression. Data from Mt. Majella were taken from Huguët et al. (2019). Data from Mts. Lautaret-Galibier were taken from Véquaud et al. (2021). Data from Mt. Shennongjia were taken from Yang et al. (2015). The global soil calibration by De Jonge et al. (2014) was applied to all these transects. Only significant regressions ($p < 0.05$) are shown.

a supprimé: 6

a supprimé: elevational

a supprimé: prediction

a supprimé: under revision

a supprimé:).

a supprimé: ,

a supprimé: t

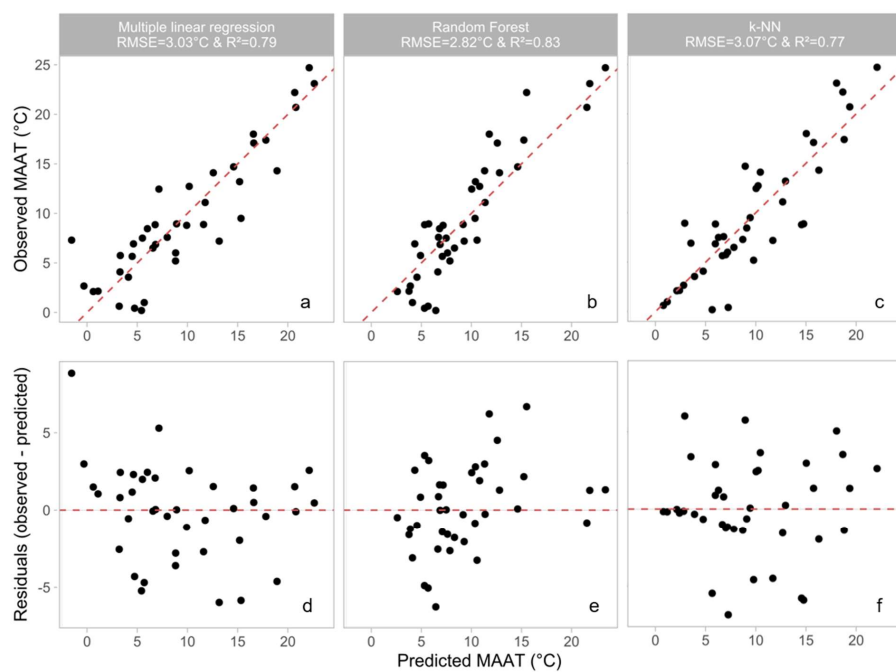


Figure 7. Results of the three different models tested to reconstruct the MAAT from 3-OH FA distribution: observed MAAT (°C) vs Predicted MAAT (°C) for (a) the multiple linear regression model, (b) the random forest model and (c) the k-NN method. MAAT residuals plotted against the predicted MAAT for (d) the multiple linear regression model, (e) the random forest model and (f) the k-NN method.

Commenté [h4]: Il faut que tu présentes tes figures 7 et 8 dans le même ordre : soit random forest en 2 et k-NN en 3, soit l'inverse.

a supprimé: ¶

a supprimé: ¶

a mis en forme : Retrait : Première ligne : 0 cm

a supprimé: (a)

a supprimé: M

a supprimé: random

a supprimé: ,

a supprimé: ,

a supprimé: .

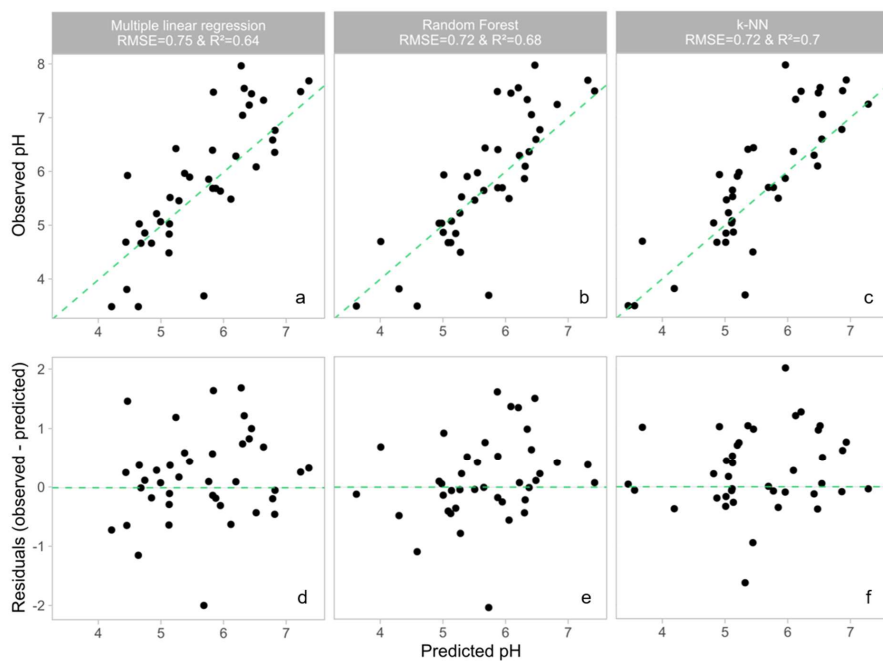


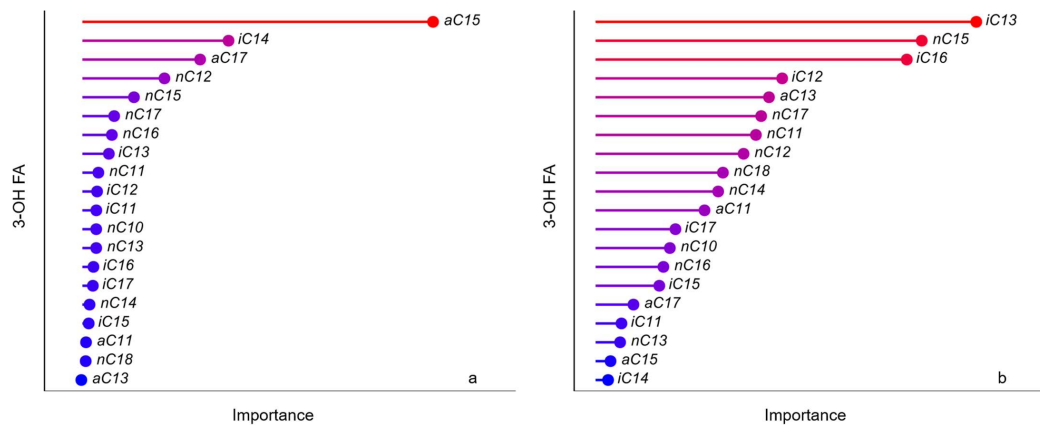
Figure 8. Results of the three different models tested to reconstruct the pH from 3-OH FA distribution: observed pH vs predicted pH for (a) the multiple linear regression model, (b) the random forest model, (c) the k-NN method. pH residuals plotted against the predicted pH for (d) the multiple linear regression model, (e) the random forest model and (f) the k-NN method.

a mis en forme : Retrait : Première ligne : 1,5 cm, Interligne : 1,5 ligne, Taquets de tabulation : 2,11 cm, Gauche

a supprimé: ¶

a supprimé:

a supprimé :



a supprimé: (a) Multiple regression, (b) k-NN method, (c) random forest.¶

Figure 9. Importance (arbitrary unit) of the 3-OH FAs used to estimate (a) MAAT and (b) pH in the random forest models proposed in this study according to the permutation importance method (Breiman, 2001).

a supprimé: values

a supprimé: values

a supprimé: ,

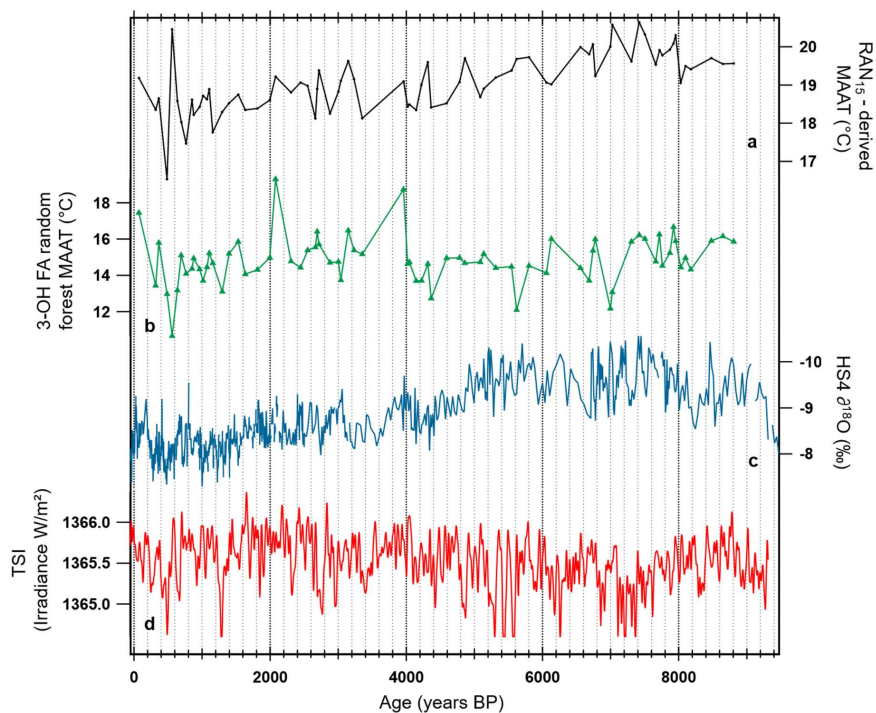


Figure 10. Comparison of the 3-OH FA model-MAAT record with other time-series and proxy records for the HS4 speleothem (Wang et al., 2018). (a) RAN₁₅-MAAT record reconstructed using a local Chinese calibration (Wang et al., 2016; Wang et al., 2018). (b) 3-OH FA random forest model-MAAT. (c) The CaCO₃ oxygen isotope record (Hu et al., 2008b). (d) Total solar irradiance (TSI; W/m²) during the Holocene (past 9300 years) based on a composite described in Steinhilber et al. (2009).

a supprimé: 9

a supprimé: 3-OH FA k-NN model-MAAT (c)

ID	Location	Altitude (m)	MAAT(°C)	pH	RAN ₁₅	RAN ₁₇	RIAN	MBT' _{5Me}	CBT'
1	Peruvian Andes	194	26.4	3.7	2.45	0.96	0.47	0.96	-1.09
2	Peruvian Andes	210	26.4	4	2.56	0.61	0.60	0.97	-1.92
3	Peruvian Andes	1063	20.7	4.7	3.46	0.70	0.54	0.98	-1.76
4	Peruvian Andes	1500	17.4	3.5	4.15	0.93	0.51	0.91	-1.55
5	Peruvian Andes	1750	15.8	3.6	5.30	1.32	0.51	0.92	-1.62
6	Peruvian Andes	1850	16	3.5	6.81	1.23	0.54	0.96	-1.76
7	Peruvian Andes	2020	14.9	3.4	7.00	1.19	0.54	0.95	-1.68
8	Peruvian Andes	2520	12.1	3.7	8.40	1.59	0.53	0.74	-1.42
9	Peruvian Andes	2720	11.1	3.6	8.42	1.73	0.48	0.83	-1.45
10	Peruvian Andes	3020	9.5	3.4	13.78	2.21	0.44	0.83	-1.21
11	Peruvian Andes	3200	8.9	3.5	6.91	2.35	0.37	0.71	-1.48
12	Peruvian Andes	3025	11.1	3.5	8.86	1.74	0.52	0.82	-1.66
13	Peruvian Andes	3400	7.7	3.4	9.10	2.39	0.40	0.71	-1.39
14	Peruvian Andes	3644	6.5	3.4	8.93	2.03	0.67	0.58	-1.21
15	Mt. Shegyla, Tibet	3106	8.9	5.53	6.22	2.02	0.51	0.59	-0.83
16	Mt. Shegyla, Tibet	3117	8.9	6.43	4.47	1.86	0.36	0.57	-0.35
17	Mt. Shegyla, Tibet	3132	8.8	6.01	4.07	1.72	0.43	0.61	-0.47
18	Mt. Shegyla, Tibet	3344	7.6	6.03	5.40	2.80	0.34	0.51	-0.67
19	Mt. Shegyla, Tibet	3355	7.5	5.87	4.09	2.71	0.23	0.44	-0.39
20	Mt. Shegyla, Tibet	3356	7.5	5.52	3.87	2.14	0.25	0.42	-0.70
21	Mt. Shegyla, Tibet	4030	3.7	5.21	8.21	3.64	0.43	0.49	-1.10
22	Mt. Shegyla, Tibet	4046	3.6	4.68	8.37	3.00	0.49	0.52	-1.17
23	Mt. Shegyla, Tibet	4050	3.6	4.61	8.94	2.47	0.50	0.44	-1.33
24	Mt. Shegyla, Tibet	3912	4.3	5.04	9.74	2.30	0.48	0.40	-2.39
25	Mt. Shegyla, Tibet	3918	4.3	4.68	8.67	1.80	0.56	0.45	-2.23
26	Mt. Shegyla, Tibet	4298	2.1	5.04	10.00	2.78	0.50	0.45	-2.04
27	Mt. Shegyla, Tibet	4295	2.2	4.87	12.17	3.90	0.50	0.42	-1.07
28	Mt. Shegyla, Tibet	4304	2.1	5.26	10.10	3.20	0.46	0.46	-1.14
29	Mt. Shegyla, Tibet	4479	1.1	5.26	10.11	3.42	0.52	0.35	-1.27
30	Mt. Shegyla, Tibet	4479	1.1	5.07	5.71	3.00	0.50	0.35	-0.84
31	Mt. Shegyla, Tibet	4474	1.1	5.24	7.88	3.65	0.42	0.32	-1.15
32	Mt. Pollino, Italy	0	18	6.78	2.71	1.19	0.15	0.50	0.31
33	Mt. Pollino, Italy	200	17	6.19	2.41	1.28	0.30	0.63	0.34
34	Mt. Pollino, Italy	400	16	6.13	4.26	2.29	0.22	0.58	0.35
35	Mt. Pollino, Italy	600	15	6.14	4.15	2.36	0.22	0.55	0.43
36	Mt. Pollino, Italy	800	14	4.53	3.34	2.77	0.34	0.51	-0.24
37	Mt. Pollino, Italy	1000	13	5.41	3.06	1.83	0.28	0.48	0.10
38	Mt. Pollino, Italy	1200	12	6.37	4.21	1.91	0.24	0.55	0.43
39	Mt. Pollino, Italy	1400	11	5.62	5.77	4.16	0.18	0.52	0.40
40	Mt. Pollino, Italy	1600	10	4.93	7.64	4.54	0.27	0.44	-0.13
41	Mt. Pollino, Italy	1800	9	4.91	3.45	3.17	0.25	0.45	-0.07
42	Mt. Pollino, Italy	2000	8	5.52	6.35	4.52	0.19	0.56	0.40
43	Mt. Pollino, Italy	2100	7.5	5.91	10.26	3.62	0.19	0.42	0.38
44	Mt. Pollino, Italy	2200	7	5.85	6.21	2.82	0.31	0.47	0.34
45	Chilean Andes	690	9.2	5.38	5.01	3.51	0.42	0.41	-0.80
46	Chilean Andes	870	8.9	5.62	5.21	2.43	0.39	0.49	-0.52
47	Chilean Andes	891	7.9	4.94	5.18	2.69	0.53	0.44	-0.94
48	Chilean Andes	915	NA	6.75	4.67	4.25	0.21	NA	NA
49	Chilean Andes	980	8.5	5.63	3.87	3.83	0.28	0.46	-0.66
50	Chilean Andes	985	5.8	4.67	6.41	3.12	0.48	0.41	-1.83
51	Chilean Andes	1125	6.0	5.00	3.83	4.18	0.46	0.42	-1.02
52	Chilean Andes	1151	6.0	5.89	4.74	2.89	0.33	0.43	-0.32
53	Chilean Andes	1196	7.1	5.79	5.70	4.07	0.34	0.43	-0.40
54	Chilean Andes	1385	NA	4.43	4.85	1.91	0.39	0.41	-2.28

Table 1. List of the soil samples collected along Mts. Shegyla, Pollino, Peruvian Andes and Chilean Andes, with corresponding altitude (m), MAAT (°C), pH and 3-OH FA/brGDGT-derived indices.

	Model	n (training)	n (test)	R ²	RMSE	Variance in residuals	Mean absolute error	Lower estimation limit	Upper estimation limit
MAAT (°C)	RAN ₁₅	-	168	0.37	5.5	29.8	4.0	-3.1	17.2
	RAN ₁₇	-	168	0.41	5.3	27.9	3.9	-4.3	17.0
	k-NN	128	40	0.77	3.1	9.4	2.3	0.5	25.0
	Multiple linear regression	128	40	0.79	3.0	9.2	2.3	-1.2	25.8
	Random forest	128	40	0.83	2.8	8.0	2.2	0.8	24.9
pH	RIAN	-	168	0.34	1.0	1.0	0.8	4.1	7.9
	k-NN	128	40	0.70	0.7	0.5	0.5	3.4	8.7
	Multiple linear regression	128	40	0.64	0.8	0.6	0.6	4.0	8.3
	Random forest	128	40	0.68	0.7	0.5	0.5	3.5	7.8

Table 2. Characteristics of the different models proposed in this study to estimate MAAT and pH; R², RMSE, variance of the residuals, mean absolute error (MAE) and the upper and lower limits of estimation. The "training" samples were used to develop the different machine learning models, which were then tested on a "test" sample set.

a supprimer: s

a supprimer:

Page 19 : [1] a supprimé	Arnaud Huguet	12/03/2021 12:18:00
--------------------------	---------------	---------------------

Page 19 : [2] a mis en forme	Arnaud Huguet	12/03/2021 13:41:00
------------------------------	---------------	---------------------

Indice

Page 19 : [3] a supprimé	Arnaud Huguet	12/03/2021 13:33:00
--------------------------	---------------	---------------------

Page 19 : [4] a supprimé	Arnaud Huguet	12/03/2021 13:42:00
--------------------------	---------------	---------------------

Page 19 : [5] a supprimé	Arnaud Huguet	12/03/2021 18:10:00
--------------------------	---------------	---------------------

Page 19 : [6] a supprimé	Arnaud Huguet	12/03/2021 18:15:00
--------------------------	---------------	---------------------

Page 19 : [7] a supprimé	Arnaud Huguet	12/03/2021 18:23:00
--------------------------	---------------	---------------------

Page 20 : [8] a supprimé	Arnaud Huguet	12/03/2021 19:21:00
--------------------------	---------------	---------------------

Page 20 : [9] a supprimé	huguet	12/03/2021 21:20:00
--------------------------	--------	---------------------

Page 20 : [9] a supprimé	huguet	12/03/2021 21:20:00
--------------------------	--------	---------------------

Page 20 : [9] a supprimé	huguet	12/03/2021 21:20:00
--------------------------	--------	---------------------

Page 20 : [9] a supprimé	huguet	12/03/2021 21:20:00
--------------------------	--------	---------------------

Page 20 : [9] a supprimé	huguet	12/03/2021 21:20:00
--------------------------	--------	---------------------

Page 20 : [9] a supprimé	huguet	12/03/2021 21:20:00
--------------------------	--------	---------------------

Page 20 : [9] a supprimé	huguet	12/03/2021 21:20:00
--------------------------	--------	---------------------

Page 20 : [10] a supprimé	huguet	12/03/2021 21:23:00
---------------------------	--------	---------------------

Page 20 : [10] a supprimé huguet 12/03/2021 21:23:00

Page 20 : [10] a supprimé huguet 12/03/2021 21:23:00

Page 20 : [11] a supprimé huguet 12/03/2021 21:46:00

Page 20 : [11] a supprimé huguet 12/03/2021 21:46:00

Page 20 : [11] a supprimé huguet 12/03/2021 21:46:00

Page 20 : [11] a supprimé huguet 12/03/2021 21:46:00

Page 20 : [12] a supprimé huguet 12/03/2021 21:54:00

Page 20 : [12] a supprimé huguet 12/03/2021 21:54:00

Page 20 : [13] a mis en forme huguet 12/03/2021 22:12:00

Indice

Page 20 : [13] a mis en forme huguet 12/03/2021 22:12:00

Indice

Page 20 : [14] a supprimé Pierre Véquaud 16/03/2021 13:24:00

Page 20 : [15] a mis en forme huguet 13/03/2021 15:42:00

Police :Italique

Page 20 : [16] a supprimé huguet 12/03/2021 21:30:00

Page 20 : [16] a supprimé huguet 12/03/2021 21:30:00

Page 20 : [17] a mis en forme huguet 12/03/2021 22:19:00

Justifié

Page 20 : [18] a mis en forme Pierre Véquaud 10/03/2021 16:35:00

Anglais (États-Unis)

Page 20 : [19] a mis en forme Pierre Véquaud 10/03/2021 16:35:00

Anglais (États-Unis)

Page 20 : [20] a mis en forme Pierre Véquaud 10/03/2021 16:35:00

Anglais (États-Unis)

Page 20 : [21] a mis en forme Pierre Véquaud 10/03/2021 16:35:00

Anglais (États-Unis)

Page 20 : [22] a mis en forme Pierre Véquaud 10/03/2021 16:35:00

Anglais (États-Unis)

Page 20 : [23] a mis en forme Pierre Véquaud 10/03/2021 16:35:00

Anglais (États-Unis)

Page 20 : [24] a mis en forme Pierre Véquaud 10/03/2021 16:35:00

Anglais (États-Unis)

Page 20 : [25] a mis en forme Pierre Véquaud 10/03/2021 16:35:00

Anglais (États-Unis)

Page 20 : [26] a mis en forme Pierre Véquaud 10/03/2021 16:35:00

Anglais (États-Unis)

Page 20 : [27] a mis en forme Pierre Véquaud 10/03/2021 16:35:00

Anglais (États-Unis)

Page 20 : [28] a supprimé Pierre Véquaud 10/03/2021 16:09:00

Page 20 : [28] a supprimé Pierre Véquaud 10/03/2021 16:09:00

Page 20 : [29] a mis en forme Pierre Véquaud 10/03/2021 16:35:00

Anglais (États-Unis)

Page 20 : [30] a mis en forme Pierre Véquaud 10/03/2021 16:35:00

Anglais (États-Unis)

Page 20 : [31] a mis en forme Pierre Véquaud 10/03/2021 16:35:00

Anglais (États-Unis)

Page 20 : [32] a mis en forme Pierre Véquaud 10/03/2021 16:35:00

Anglais (États-Unis)

Page 20 : [33] a mis en forme Pierre Véquaud 10/03/2021 16:35:00

Anglais (États-Unis)

Page 20 : [34] a mis en forme Pierre Véquaud 10/03/2021 16:35:00

Anglais (États-Unis)

Page 20 : [35] a mis en forme Pierre Véquaud 10/03/2021 16:35:00

Anglais (États-Unis)

Page 20 : [36] a mis en forme Pierre Véquaud 10/03/2021 16:35:00

Anglais (États-Unis)

Page 20 : [37] a mis en forme Pierre Véquaud 10/03/2021 16:35:00

Anglais (États-Unis)

Page 20 : [38] a mis en forme Pierre Véquaud 10/03/2021 16:35:00

Anglais (États-Unis)

Page 20 : [38] a mis en forme Pierre Véquaud 10/03/2021 16:35:00

Anglais (États-Unis)

Page 20 : [39] a mis en forme Pierre Véquaud 10/03/2021 16:35:00

Anglais (États-Unis)

Page 20 : [40] a mis en forme Pierre Véquaud 10/03/2021 16:35:00

Anglais (États-Unis)

Page 20 : [41] a mis en forme Pierre Véquaud 10/03/2021 16:35:00

Anglais (États-Unis)

Page 20 : [42] a mis en forme Pierre Véquaud 10/03/2021 16:35:00

Anglais (États-Unis)

Page 20 : [43] a mis en forme Pierre Véquaud 10/03/2021 16:35:00

Anglais (États-Unis)

Page 20 : [44] a mis en forme Pierre Véquaud 10/03/2021 16:35:00

Anglais (États-Unis)

Page 20 : [45] a mis en forme Pierre Véquaud 10/03/2021 16:35:00

Anglais (États-Unis)

Page 20 : [46] a supprimé huguet 12/03/2021 22:19:00

Page 20 : [47] a supprimé huguet 12/03/2021 22:21:00

▲ Page 20 : [48] a supprimé huguet 12/03/2021 22:23:00

▼
▲ Page 20 : [48] a supprimé huguet 12/03/2021 22:23:00

▼
▲ Page 20 : [49] a supprimé Pierre Véquaud 10/03/2021 13:52:00

▼
▲ Page 20 : [49] a supprimé Pierre Véquaud 10/03/2021 13:52:00

▼
▲ Page 20 : [49] a supprimé Pierre Véquaud 10/03/2021 13:52:00

▼
▲ Page 20 : [49] a supprimé Pierre Véquaud 10/03/2021 13:52:00

▼
▲ Page 20 : [50] a supprimé huguet 12/03/2021 22:25:00

▼
▲ Page 20 : [50] a supprimé huguet 12/03/2021 22:25:00

▼
▲ Page 20 : [51] a mis en forme huguet 12/03/2021 22:42:00

Indice ←

▲ Page 20 : [51] a mis en forme huguet 12/03/2021 22:42:00

Indice ←

▲ Page 20 : [52] a supprimé Pierre Véquaud 16/03/2021 16:14:00

▼
▲ Page 20 : [52] a supprimé Pierre Véquaud 16/03/2021 16:14:00

▼
▲ Page 20 : [52] a supprimé Pierre Véquaud 16/03/2021 16:14:00

▼
▲ Page 20 : [52] a supprimé Pierre Véquaud 16/03/2021 16:14:00

▼
▲ Page 20 : [53] a mis en forme huguet 12/03/2021 22:44:00

Indice ←

▲ Page 20 : [53] a mis en forme huguet 12/03/2021 22:44:00

Indice

Page 21 : [54] a supprimé huguet 12/03/2021 22:51:00

Page 21 : [54] a supprimé huguet 12/03/2021 22:51:00

Page 21 : [55] a mis en forme huguet 13/03/2021 13:26:00
Police :Italique

Page 21 : [55] a mis en forme huguet 13/03/2021 13:26:00
Police :Italique

Page 21 : [55] a mis en forme huguet 13/03/2021 13:26:00
Police :Italique

Page 21 : [55] a mis en forme huguet 13/03/2021 13:26:00
Police :Italique

Page 21 : [55] a mis en forme huguet 13/03/2021 13:26:00
Police :Italique

Page 21 : [55] a mis en forme huguet 13/03/2021 13:26:00
Police :Italique

Page 21 : [55] a mis en forme huguet 13/03/2021 13:26:00
Police :Italique

Page 21 : [55] a mis en forme huguet 13/03/2021 13:26:00
Police :Italique

Page 21 : [55] a mis en forme huguet 13/03/2021 13:26:00
Police :Italique

Page 21 : [55] a mis en forme huguet 13/03/2021 13:26:00
Police :Italique

Page 21 : [55] a mis en forme huguet 13/03/2021 13:26:00
Police :Italique

Page 21 : [55] a mis en forme huguet 13/03/2021 13:26:00
Police :Italique

Page 21 : [55] a mis en forme huguet 13/03/2021 13:26:00
Police :Italique

Page 21 : [55] a mis en forme	huguet	13/03/2021 13:26:00
-------------------------------	--------	---------------------

Police :Italique

Page 21 : [55] a mis en forme	huguet	13/03/2021 13:26:00
-------------------------------	--------	---------------------

Police :Italique

Page 21 : [55] a mis en forme	huguet	13/03/2021 13:26:00
-------------------------------	--------	---------------------

Police :Italique

Page 21 : [56] a supprimé	derennes	15/03/2021 18:37:00
---------------------------	----------	---------------------

Page 21 : [56] a supprimé	derennes	15/03/2021 18:37:00
---------------------------	----------	---------------------

Page 21 : [57] a mis en forme	huguet	13/03/2021 14:47:00
-------------------------------	--------	---------------------

Indice

Page 21 : [57] a mis en forme	huguet	13/03/2021 14:47:00
-------------------------------	--------	---------------------

Indice

Page 21 : [57] a mis en forme	huguet	13/03/2021 14:47:00
-------------------------------	--------	---------------------

Indice

Page 21 : [57] a mis en forme	huguet	13/03/2021 14:47:00
-------------------------------	--------	---------------------

Indice

Page 21 : [57] a mis en forme	huguet	13/03/2021 14:47:00
-------------------------------	--------	---------------------

Indice

Page 21 : [57] a mis en forme	huguet	13/03/2021 14:47:00
-------------------------------	--------	---------------------

Indice

Page 21 : [57] a mis en forme	huguet	13/03/2021 14:47:00
-------------------------------	--------	---------------------

Indice

Page 21 : [57] a mis en forme	huguet	13/03/2021 14:47:00
-------------------------------	--------	---------------------

Indice

Page 21 : [57] a mis en forme	huguet	13/03/2021 14:47:00
-------------------------------	--------	---------------------

Indice

Page 21 : [57] a mis en forme	huguet	13/03/2021 14:47:00
-------------------------------	--------	---------------------

Indice

Page 21 : [58] a mis en forme	huguet	13/03/2021 15:11:00
-------------------------------	--------	---------------------

Indice

Page 21 : [58] a mis en forme huguet 13/03/2021 15:11:00
Indice

Page 21 : [58] a mis en forme huguet 13/03/2021 15:11:00
Indice

Page 21 : [58] a mis en forme huguet 13/03/2021 15:11:00
Indice

Page 21 : [59] a supprimé huguet 13/03/2021 12:07:00

Page 21 : [60] a mis en forme huguet 13/03/2021 12:25:00
Indice

Page 21 : [60] a mis en forme huguet 13/03/2021 12:25:00
Indice

Page 21 : [61] a supprimé huguet 13/03/2021 12:25:00

Page 21 : [61] a supprimé huguet 13/03/2021 12:25:00

Page 21 : [62] a mis en forme huguet 13/03/2021 15:55:00
Indice

Page 21 : [62] a mis en forme huguet 13/03/2021 15:55:00
Indice

Page 22 : [63] a supprimé huguet 13/03/2021 15:22:00

Page 22 : [64] a mis en forme Pierre Véquaud 10/03/2021 16:21:00
Anglais (États-Unis)

Page 22 : [65] a mis en forme huguet 13/03/2021 15:23:00
Retrait : Première ligne : 0 cm

Page 22 : [66] a mis en forme huguet 13/03/2021 15:42:00
Police :Italique

Page 22 : [67] a mis en forme huguet 13/03/2021 15:51:00
Retrait : Première ligne : 1,25 cm

Page 22 : [68] a supprimé huguet 13/03/2021 15:25:00

Page 22 : [68] a supprimé huguet 13/03/2021 15:25:00

Page 22 : [69] a supprimé huguet 13/03/2021 15:36:00

Page 22 : [69] a supprimé huguet 13/03/2021 15:36:00

Page 22 : [69] a supprimé huguet 13/03/2021 15:36:00

Page 22 : [70] a mis en forme huguet 13/03/2021 15:38:00

Justifié

Page 22 : [71] a supprimé huguet 13/03/2021 15:36:00

Page 22 : [71] a supprimé huguet 13/03/2021 15:36:00

Page 22 : [72] a supprimé Pierre Véquaud 10/03/2021 16:14:00

Page 22 : [72] a supprimé Pierre Véquaud 10/03/2021 16:14:00

Page 22 : [73] a mis en forme Pierre Véquaud 10/03/2021 16:15:00

a mis en forme

Page 22 : [74] a mis en forme Pierre Véquaud 10/03/2021 16:15:00

a mis en forme

Page 22 : [75] a supprimé huguet 13/03/2021 15:37:00

Page 22 : [75] a supprimé huguet 13/03/2021 15:37:00

Page 22 : [76] a supprimé Pierre Véquaud 10/03/2021 16:16:00

Page 22 : [76] a supprimé Pierre Véquaud 10/03/2021 16:16:00

Page 22 : [77] a supprimé huguet 13/03/2021 15:40:00

▲ Page 22 : [77] a supprimé huguet 13/03/2021 15:40:00

▼
▲ Page 22 : [78] a supprimé Pierre Véquaud 10/03/2021 13:19:00

▼
▲ Page 22 : [78] a supprimé Pierre Véquaud 10/03/2021 13:19:00

▼
▲ Page 22 : [79] a supprimé huguet 13/03/2021 15:38:00

▼
▲ Page 22 : [79] a supprimé huguet 13/03/2021 15:38:00

▼
▲ Page 22 : [80] a supprimé huguet 13/03/2021 15:53:00

▼
▲ Page 22 : [80] a supprimé huguet 13/03/2021 15:53:00

▼
▲ Page 22 : [81] a mis en forme huguet 13/03/2021 16:04:00

Exposant

▲ Page 22 : [82] a mis en forme huguet 13/03/2021 16:16:00

Police :Italique

▲ Page 22 : [82] a mis en forme huguet 13/03/2021 16:16:00

Police :Italique

▲ Page 22 : [82] a mis en forme huguet 13/03/2021 16:16:00

Police :Italique

▲ Page 22 : [82] a mis en forme huguet 13/03/2021 16:16:00

Police :Italique

▲ Page 22 : [82] a mis en forme huguet 13/03/2021 16:16:00

Police :Italique

▲ Page 22 : [82] a mis en forme huguet 13/03/2021 16:16:00

Police :Italique

▲ Page 22 : [82] a mis en forme huguet 13/03/2021 16:16:00

Police :Italique

▲ Page 22 : [82] a mis en forme huguet 13/03/2021 16:16:00

Police :Italique

Page 22 : [82] a mis en forme huguet 13/03/2021 16:16:00

Police :Italique

Page 22 : [82] a mis en forme huguet 13/03/2021 16:16:00

Police :Italique

Page 22 : [83] a supprimé huguet 13/03/2021 15:55:00

Page 22 : [84] a supprimé huguet 13/03/2021 16:05:00

Page 22 : [85] a mis en forme huguet 13/03/2021 17:21:00

Retrait : Première ligne : 1,43 cm

Page 22 : [86] a mis en forme Pierre Véquaud 10/03/2021 14:37:00

Anglais (États-Unis)

Page 22 : [86] a mis en forme Pierre Véquaud 10/03/2021 14:37:00

Anglais (États-Unis)

Page 22 : [87] a mis en forme Pierre Véquaud 10/03/2021 14:37:00

Anglais (États-Unis)

Page 22 : [87] a mis en forme Pierre Véquaud 10/03/2021 14:37:00

Anglais (États-Unis)

Page 22 : [87] a mis en forme Pierre Véquaud 10/03/2021 14:37:00

Anglais (États-Unis)

Page 22 : [88] a supprimé huguet 13/03/2021 16:32:00

Page 22 : [89] a supprimé derennes 15/03/2021 18:49:00

Page 22 : [89] a supprimé derennes 15/03/2021 18:49:00

Page 23 : [90] a supprimé huguet 13/03/2021 17:27:00

Page 23 : [91] a supprimé derennes 15/03/2021 09:50:00

Page 23 : [92] a supprimé huguet 13/03/2021 17:40:00

Page 23 : [93] a supprimé	huguet	13/03/2021 17:41:00
---------------------------	--------	---------------------

Page 23 : [94] a supprimé	huguet	13/03/2021 17:43:00
---------------------------	--------	---------------------

Page 23 : [95] a supprimé	huguet	13/03/2021 17:48:00
---------------------------	--------	---------------------

Page 25 : [96] a supprimé	huguet	13/03/2021 18:52:00
---------------------------	--------	---------------------

Page 25 : [97] a supprimé	huguet	13/03/2021 19:13:00
---------------------------	--------	---------------------